39th AIAA Fluid Dynamics Conference
22 - 25 June 2009, San Antonio, Texas

AIAA 2009-4030

Experimental Investigation of Pitching and Plunging Airfoils at Reynolds Number between 1×10^4 and 6×10^4

Yeon Sik Baik* , Jonathan M. Rausch† , and Luis P. Bernal‡
University of Michigan, Ann Arbor, MI

Michael V. Ol§
Air Force Research Lab, Wright-Patterson AFB

An experimental investigation was performed on a nominally two-dimensional pitching and plunging SD7003 and flat plate at Reynolds number 1×10^4, 3×10^4, and 6×10^4. The experiment was conducted at the University of Michigan water channel facility using phase-averaged particle image velocimetry (PIV) technique to quantify the flow field. Two sets of airfoil kinematics were used in this study; a combined pitching and plunging motion, and a pure plunging motion. The flow topology and wall velocity profiles from the PIV measurements showed a Re dependence on a pitching and plunging SD7003 where the extent of flow separation is reduced at a relatively high Re. On the contrary, flat plate displayed a large leading edge separation flow characteristic that was independent of Re. For both airfoil cross-sections used in the experiment, turbulence statistics indicated laminar to turbulent transition phenomena at low Re. The study shows the leading edge shape effect on the flow transition and separation characteristics. A pure plunging motion of SD7003 and flat plate at Re = 60,000 showed the formation of the leading and trailing edge vortices. In addition, a quantitative analysis showed an apparent phase lag present on SD7003 relative to the flat plate. In order to validate the experimental data, a flow comparison between the University of Michigan and AFRL was performed.

Nomenclature

c = Chord [m]
f = Motion frequency [1/s]
h_0 = Normalized plunge amplitude [1]
k = $\pi f c/U_\infty$,Reduced frequency [1]
Re = Reynolds number [1]
St = $2kh_0/\pi$,Strouhal number [1]
t = Time [s]
U_∞ = Free stream velocity [m/s]
x_p = Chordwise location of the center of rotation [m]

α_0 = Mean angle of attack [1]
α_{eff} = Effective angle of attack [1]
ω^* = Normalized vorticity [1]
θ_0 = Pitch amplitude [1]
ϕ = Phase lag [1]

*Graduate Research Assistant, University of Michigan, Department of Aerospace Engineering, yeonb@umich.edu
†Graduate Research Assistant, University of Michigan, Department of Aerospace Engineering, rauschjm@umich.edu
‡Associate Professor, University of Michigan, Department of Aerospace Engineering, lpb@umich.edu
§Aerospace Engineer, Air Vehicles Directorate, Wright-Patterson AFB, OH Michael.Ol@wpafb.af.mil

This material is declared a work of the U.S. Government and is not subject to copyright protection in the United States.

I. Introduction

THIS paper presents the results of an experimental investigation on the aerodynamics of pitching and plunging airfoils. The research is motivated by recent interests on the aerodynamics of flapping wings for application to Micro Air Vehicle (MAV) flight. A recent review of biological fly and flapping wing aerodynamics is provided by Shyy *et al.*[1] In contrast to earlier studies of unsteady airfoils, the aerodynamics of flapping wings is characterized by large amplitude pitching and plunging motions of the wing at relatively low Reynolds number. At these flow conditions large scale vortices at the leading edge and trailing edge are observed during the motion.[2] The formation of a leading edge vortex is a feature also found in helicopter blade aerodynamics, which produces the high lift coefficients associated with dynamic stall.[3] Formation of leading edge and trailing edge vortices are prominent features in the aerodynamics of biological fliers[1] and are believe to be critical to force generation. Because of low Reynolds number, laminar-to-turbulent transition is expected to play an important role in the flow dynamics of small flapping-wing fliers. Elucidating the interplay between unsteady boundary layer separation and reattachment, leading edge and trailing edge vortex formation, and laminar to turbulent transition as a function of Reynolds number is the main objective of the present research.

A second objective of the present effort is to obtain comprehensive flow field data for validation of computational and theoretical analyses of these flows. Flow visualization and Particle Image Velocimetry (PIV) velocity field measurements, including second order statistics, are reported here. A companion paper[4] reports detailed comparisons of the present experimental measurements with numerical simulations of the same flows. Two airfoil cross sections are considered: a SD7003 and a 2.3%-thick flat plate with rounded leading and trailing edges. The SD7003 airfoil is investigated because it has been extensively studied at a wide range of Reynolds numbers.[5] We consider also a flat plate airfoil because it is more representative of airfoil sections found in low Reynolds number biological flyers. Both airfoil sections are investigated with two motion kinematics. In one case we consider combined pitching and plunging sinusoidal motion with effective angle of attack varying in the range 2.4° to 13.6° . Here we define the effective angle of attack as the airfoil angle of attack in the frame of reference translating with the center of rotation of the airfoil ($x/c = 0.25$). In the second case the airfoil kinematics consists of pure plunge motion with effective angle in the range -6° to 22°. The SD7003 stall angle of attack for steady flow is at 11°, and therefore the above kinematics include mild and deep stall flow conditions, respectively. All the experiments are conducted at Reynolds numbers in the range 1×10^4 and 6×10^4. Initial results for the SD7003 airfoil, not including second order statistics, were reported in Kang *et al.*[6] An extensive study of the SD7003 airfoil in pitching and plunging motion including flow visualization results and PIV measurements has been reported by Ol *et al*[2] and selected results will be included here for comparison.

II. Experimental Setup

Experiments were conducted in two facilities: the Horizontal Free-surface Water Tunnel (HFWT) at the Air Force Research Laboratory (AFRL) and the low-turbulence water channel at the University of Michigan (UM). The low-turbulence water channel at the University of Michigan has a test cross-section of 61cm wide by 61cm high, and is capable of generating free stream velocity ranging from 5 cm/s to 40 cm/s with a turbulence intensity of approximately 1%. The turbulence intensity was measured by taking PIV images in the free stream for a period comparable to the duration of the unsteady tests, of the order of hours, while maintaining the water channel operating at a constant motor speed. The short time turbulence intensity computed by averaging over a time period of the order of the test section residence time is less than 0.5%, significantly lower than the long time average. The larger value of the long time average is associated with very low frequency sloshing in the facility. The HFWT at AFRL test section is 46cm wide by 61cm high and the speed range is 3 cm/s to 45 cm/s. The HFWT's free stream turbulence intensity is approximately 0.5%.

A SD7003 airfoil and flat plate model with approximately 152mm chord were tested in both facilities. UM SD7003 airfoil model was fabricated using stereo lithography and a transparent resin (DSM Somos 11122) to minimize laser reflection at the surface of the airfoil. AFRL SD7003 airfoil was wire-cut from five 10cm blocks of 316-series stainless steel to a shell thickness of 0.89mm, and the blocks were welded edge-to-edge to form the full model. The flat plate model used in both facilities was fabricated from stainless steel with the same chord and span dimensions used in SD7003. UM flat plate had a polished surface that minimized

the diffuse reflection from the laser beam, hence reducing the glare near the surface. The wingspan of AFRL model was shorter than UM model due to the difference in mounting scheme. Both models spanned the water channel test section and the distance between the model and the wall was approximately 1 mm.

In the low-turbulence water channel at UM the model is mounted vertically, with the span axis normal to the water free surface. An end plate attached to the model is used to minimize free surface effects. This mounting scheme allows flexibility in the model since the model is only supported at one end. This cantilevered mounting scheme results in more flexibility in the model since it is only supported at one end. The maximum deflection of the wing tip at the highest Re tested was approximately 0.5cm and 0.1cm for the SD7003 and flat plate models, respectively. In the HFWT at AFRL the model is mounted horizontally supported by a vertical strut that connects to the mid-span on the airfoil pressure side. A slight disadvantage of horizontal mounting scheme is the strut interference with the flow field. As will be shown in the results section the differences in mounting scheme and overall dimension do not affect the flow about the models in a significant way.

The two experimental facilities implement different flow visualization systems. The flow visualization system used in the University of Michigan water channel consists of seven uniformly distributed dye streams introduced half chord in front of the leading edge of the model. Two syringe pumps are used to adjust the dye speed at the injection point in order to match the water channel flow speed and minimize disturbances produced by the wake of the dye injection system. The dye streams are held fixed and the airfoil is pitched and plunged within the width of the dye streams. The resulting streakline flow visualization pictures capture flow direction and recirculation zones. The AFRL flow visualization system consists of two cross-flow dye streams inserted at the leading edge of the model as shown in Figure 1. The dye speed is 30% of the free stream velocity. In this case the dye is a tracer for vorticity introduced at the leading edge, and provides a somewhat different yet complementary view of the flow field compared to the UM flow visualization system.

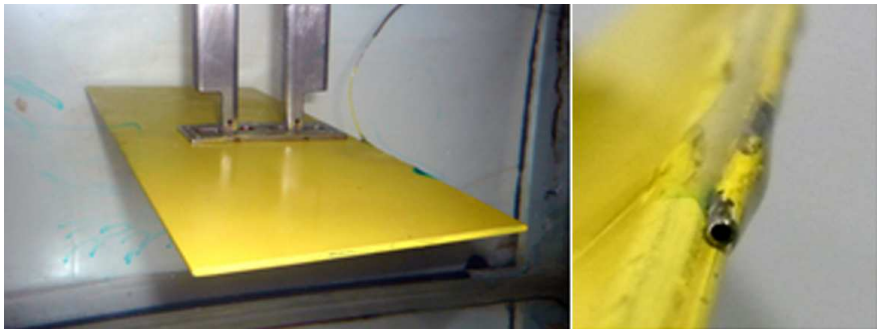

Figure 1. Flat plate model and attached dye injection system used in AFRL HFWT

The PIV system at the University of Michigan includes a double-pulsed Nd-YAG laser (Spectra Physics PIV 300), light sheet formation optics, two dual frame digital cameras (Cooke Corp. PCO-4000), computer image acquisition system and control electronics. The airfoil motion is produced by a rotary stage (Velmex B4872TS Rotary Table) for the pitch motion , a linear traverse (Velmex 20-inch BiSlide) for the plunge motion, a linear traverse (Velmex 40-inch BiSlide) for the axial motion, and the associated computer control system (Velmex VXM-1-1 motor control). The experimental setup is illustrated in Figure 2.

For PIV image acquisition, the water channel was seeded with 3-μm diameter Titanium Dioxide particles. A small amount (8 drops) of a dispersant (DARVAN C-N, Vanderbilt) was used to produce a uniform distribution of particles and to help maintain the particles in suspension for long periods of time of the order of several days. The cameras were installed underneath the water channel test section and were equipped with Nikon 105-mm Micro-Nikkor lenses to produce a magnification of approximately 25 pixels/mm. With this magnification the time between exposures was adjusted to produce a nominal particle displacement of 8 pixels at the free stream velocity in all cases. The PCO-4000 camera frame size is 4008 by 2672 pixels, which for the present magnification corresponds to 160 by 107 mm in the flow. The airfoil plunge motion was exactly 152 mm, or 1 chord length of the model. In order to capture the large amplitude motion and to avoid shadowing of the field of view, the PIV images were obtained in four separate tests for each flow condition. In two tests the leading edge region were imaged, and in the other two tests the trailing edge region were imaged. For the leading or trailing edge imaging experiments two tests were conducted, one capturing the extreme plunge motion locations (phases) with the two PCO-4000 cameras positioned side by

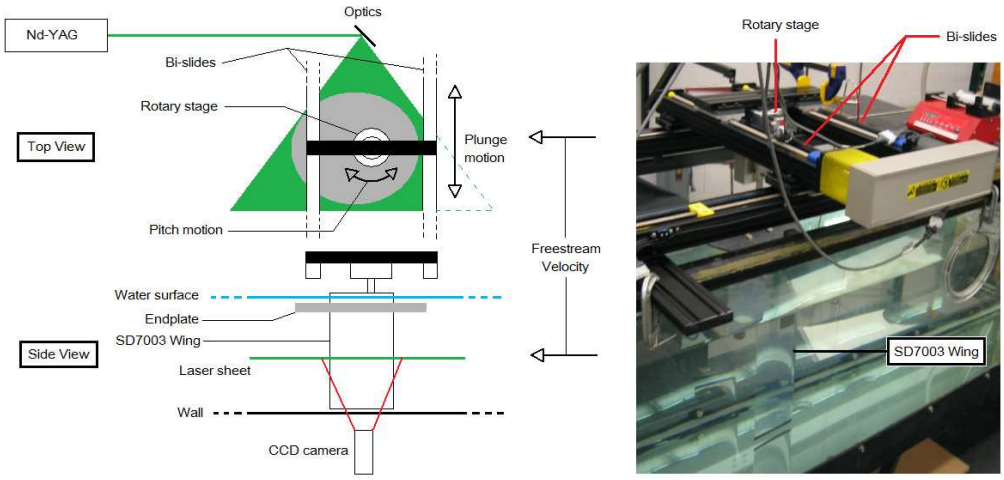

Figure 2. PIV setup in water channel facility at the University of Michigan

side; and the other capturing the center locations of the plunge motion with only one camera. To ensure smooth image processing, the leading and trailing edge images contained an overlap region. The accuracy of the overlap region was directly linked to the accuracy of the traverse system. The accuracy of the axial Velmex BiSlide traverse is 0.00635 mm, which corresponds to approximately 1/6 of a pixel for the present magnification.

In the present measurements the velocity field at specific phases of the airfoil motion were recorded and used to calculate phase-averaged mean flow fields. A total of 200 images were taken at each phase. The Nd-YAG laser, CCD cameras, rotary stage, and BiSlide were precisely synchronized to capture the desired phases of the motion. Every experiment recorded 12 cycles of the motion and only the last 10 used to compute the phase averages. Recording was initiated by the PIV system data acquisition, which triggered the motion controller. The PIV laser pulse period and the motion period were matched with an accuracy of 0.1 ms for a typical period of approximately 10 s. This produced a slight discrepancy in the model position between the first image and the last image at phases with large speed motion. The maximum shift displacement for all cases was approximately 7 pixels, which corresponds to 0.28 millimeters. In terms of data processing, this discrepancy resulted in an elimination of a datum point near the model surface.

The PIV images were analyzed using an in-house developed MATLAB-based PIV analysis software. The particle displacement is determined in two passes using cross-correlation analysis of displaced interrogation windows. The location of the cross-correlation peak, which gives the particle displacement, is measured with sub-pixel resolution using a Gaussian fit of the cross correlation function around the peak. In the first low-resolution pass a fixed displacement of 8 pixels and an interrogation window of 64 by 64 pixel were used; in the second high-resolution pass the particle displacement measured in the first pass and an interrogation window size of 32 by 32 pixels were used. This corresponds to an approximate spatial resolution of the PIV measurements of 0.64 mm. Several validation criteria were applied to the measured particle displacements. The peak magnitude must be at least three standard deviations above the mean of the cross-correlation function; and the displacement must be within a predetermined range of values in the x- and y-directions. The range of values in the first pass is fairly large to capture the large range of particle displacements found near the model surface; and small (10 pixels displacement) in the second pass. A median filter is used to find the particle displacement at the points where the PIV validation failed, and to remove outliers. A square grid with 16 pixel spacing was used for all the images. Near the surface of the airfoil, data points within 32 pixels from the boundary were discarded because the interrogation window would include pixels in the model. This corresponds to two data points in the measurement grid.

Turbulence statistics were computed at each phase using 200 processed PIV image pairs. The median filter used in the PIV processing step removed outliers based on velocity vector values on spatially adjacent points. To further remove outliers based on large sample-to-sample fluctuations a 3-sigma filter was implemented. The sample mean and standard deviation from processed PIV data were calculated at a particular point in the flow field. With the calculated mean and standard deviation value, each datum point was revisited and

the value was compared to ±3 standard deviation of the mean value. The datum point was discarded if it lied outside the 3-sigma region and the number of images remaining were recorded to calculate more accurate total number of images used in the statistics. Out of 200 images recorded, approximately 195 images were used for turbulence statistics for a relatively attached flow fields. For large separated flows approximately 180 images, or 90% of the images were retained after the 3-sigma filter. The calculated 95% confidence interval for the UM PIV data set is tabulated in Table 1.

	Pitching and plunging						Pure plunging	
95% Confidence Interval	SD7003 (Re = 10k)		SD7003 (Re = 30k, 60k)		Flat Plate (Re = 10k, 30k, 60k)		SD7003 + Flat Plate (Re = 60k)	
	mean	max	mean	max	mean	max	mean	max
u,v (% error of U_∞)	∼±1.5%	∼±5%	∼±0.5%	∼±7%	∼±1.5%	∼±7%	∼±2%	∼±9%
$\overline{u'^2}$,$\overline{v'^2}$,$\overline{u'v'}$ (% error of U_∞^2)	∼±0.07%	∼±0.42%	∼±0.01%	∼±0.53%	∼±0.07%	∼±0.7%	∼±0.13%	∼±1.25%

Table 1. Summary of 95% confidence interval for all PIV measurements taken at UM

In Table 1 the values of the 95% confidence intervals (CIs) are normalized. The primitive variables, such as u, are normalized by U_∞. For the 2nd order statistics, such as $\overline{u'v'}$, are normalized by U_∞^2. For each case two values of the 95% confidence interval are reported; the mean and the maximum. The mean is the mean of the 95% confidence intervals computed for all the phases in a particular case. The maximum simply reports the maximum 95% confidence interval in the entire flow field for all phases. This value indicates the worst possible uncertainty on the calculated mean value for a given airfoil kinematics. The mean and the maximum 95% confidence intervals were computed for pitching and plunging, and pure plunging cases at all Re. The cases with similar CIs were combined into a single category and it is tabulated in Table 1.

In general, the mean and the maximum CIs at phase 0° and 270° were an order of magnitude less than other phases. This was to be expected due to attached flow characteristics at these phases. For the same reason, SD7003 undergoing pitching and plunging motion at Re = 30,000 and 60,000 had smaller CIs than flat plate undergoing the same motion. The CIs for the pitching and plunging SD7003 at Re = 10,000 was closer to the flat plate cases. The greatest error was found for pure plunging motion due to larger turbulent separated flow regions observed at each phase.

	UM	AFRL
Test section height (cm)	61	61
Test section width (cm)	61	46
SD7003 airfoil chord (cm)	15.2	15.24
SD7003 airfoil span (cm)	60.0	45.7
Flat plate chord (cm)	15.2	15.24
Flat plate span (cm)	60.1	45.7
Wall-to-airfoil gap (cm)	<0.1	<0.1
Particle seeding	3 micron diameter TiO_2	2 - 3 micron diameter TiO_2
Freestream turbulence intensity	<1%	0.4 –0.5%

Table 2. Similarity and differences of two facilities

In summary, the experimental setup in AFRL is not vastly different from those at UM, but there are a few notable differences in the setup. Apart from the differences in the mounting scheme, the equipment used to produce airfoil motions in the AFRL water tunnel introduces less model vibration because of much finer steps in the motion. The differences in the PIV image processing software were validated by cross-processing the data for a few number of images, but the consistency between the 2 software is still in question. A detailed experimental setup and PIV procedures at AFRL can be found from Ol *et al.*[2] A short summary highlighting the similarity and differences between the 2 facilities is tabulated in Table 2.

III. Results

The airfoil motions considered in this study consist of sinusoidal pitching and plunging motions of the same frequency. Equations of motion for pitching and plunging are shown in Equation (1) and (2), respectively.

$$\theta(t) = \alpha_0 + \theta_0 \cos(2\pi f t + \phi) \tag{1}$$

$$h(t) = h_0 c \cos(2\pi f t) \tag{2}$$

$\theta(t)$ is the airfoil pitch angle where α_0 is the mean pitch angle, θ_0 is the pitch oscillation amplitude, $h(t)$ is the vertical location of the pivot point, h_0 is the normalized plunge amplitude, f is the physical frequency of the motion and ϕ is the phase lag between the pitch and plunge motions. The effective angle of attack is the angle of attack in the frame of reference moving with the center of rotation, shown in Equation (3).

$$\alpha_{\text{eff}}(t) = \alpha_0 + \theta_0 \sin(2\pi f t) + \arctan(\pi St \sin(2\pi f t)) = \alpha_0 + \alpha_{\text{pitch}} + \alpha_{\text{plunge}} \tag{3}$$

$St = 2fch_0/U_\infty$ is the Strouhal number. For St less than 0.12, $\arctan(\pi St \sin(2\pi f t))$ can be approximated as $\pi St \sin(2\pi f t)$. However, for St greater than 0.12, the arctangent function can no longer be approximated with small angle assumption and hence the resulting $\alpha_{\text{eff}}(t)$ will not be sinusoidal.

In this investigation we consider two motion kinematics: a combined pitching and plunging motion and a pure plunging motion. The motion paraters are listed in 3. For the combined pitching an dplunging motion the phase lag of 90° was chosen in order to produce sinusoidal effective angle of attack, $\alpha_{\text{eff}}(t)$.

Parameters	Pitching and Plunging	Pure Plunging
α_0	8°	8°
θ_0	-8.42°	0°
h_0	0.5	0.5
k	0.25	0.25
St	0.08	0.08
x_p	0.25c	–
ϕ	$\pi/2$ rad or 90°	$\pi/2$ rad or 90°

Table 3. List of parameters for pitching and plunging airfoil motion

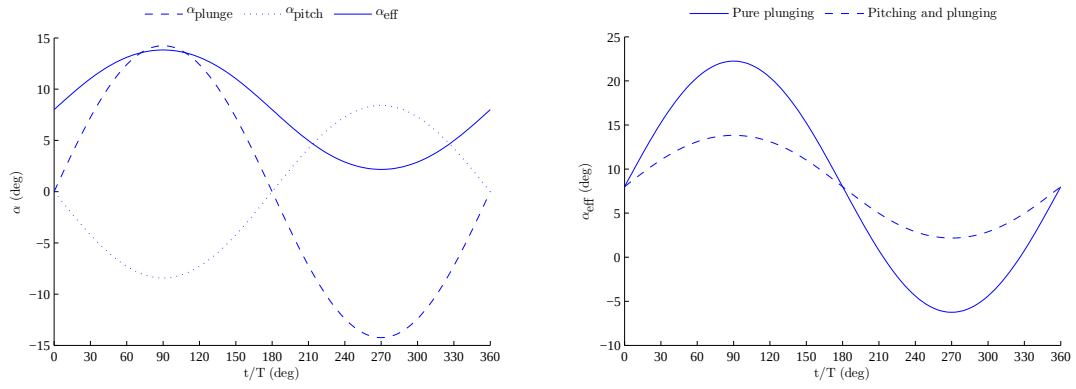

(a) (b)

Figure 3. $\alpha(t)$ of pitching and plunging motion (LEFT), and Pure plunging case induces higher α_{eff} (RIGHT)

Figure 3(a) illustrates the components and the effective angle of attack time history for pitching and plunging motion. $\alpha_{\text{eff}}(t)$ is approximately sinusoidal since St is 0.08. The resulting effective angle of attack amplitude is 5.62° which results in $\alpha_{\text{eff(max)}} = 13.62°$ and $\alpha_{\text{eff(min)}} = 2.38°$. Figure 3(b) compares $\alpha_{\text{eff}}(t)$

of pitching and plunging motion against pure plunging motion. The $\alpha_{\text{eff(max)}}$ for pure plunging motion was exactly 8.42° higher than pitching and plunging $\alpha_{\text{eff(max)}}$ due to the absence of offset motion produced by the pitching airfoil. The range of α_{eff} for pure plunging motion ranged from -6.04° to 22.04°.

A. SD7003: Pitching and plunging motion

Figure 4 shows side-by-side comparison of UM dye flow visualization, PIV velocity field data (phase averaged u-component) and PIV vorticity field data (phase averaged out-of-plane component) for the pitching and plunging SD7003 at $Re = 10{,}000$. Figure 5 shows PIV phase averaged vorticity field and the phase average turbulence statistics (normalized $\overline{u'^2}$, $\overline{v'^2}$ and $\overline{u'v'}$ correlations). The incoming free stream velocity at $Re =$ 10,000 is 6.7 cm/s and the period of the motion is approximately 28s. There is excellent correlation between the flow visualization results and the flow field data. At phase 0° the boundary layer flow is laminar and attached except perhaps towards the trailing edge of the airfoil. At phase 90° the boundary layer separates and transitional vertical structures are observed on the suction side of the airfoil. Note that these flow structures persist through the phase average process indicating that the flow disturbances are synchronized with the airfoil motion. The 2nd order statistics show relatively large values of $\overline{u'^2}$ and $\overline{v'^2}$ at the center of the transitional flow features. The $\overline{u'v'}$ correlation values remain relatively small until the $x/c \approx 0.75$. The flow at phases 120° through 180° shows similar features. There is boundary layer separation near the leading edge with some vortical features observed in the initial development of the shear layer. These features are again phase locked with the airfoil motion but they are not as coherent as at phase 90°. At these phases the separated shear layer transitions to turbulent flow very rapidly ($x/c \approx 0.2$) and the $\overline{u'v'}$ correlations are consistent with strong mixing and highly three-dimensional flow in the separated shear layer. There is significant anisotropy in the separated shear layer with $\overline{u'^2}$ values significantly larger than $\overline{v'^2}$ values. Finally at phase 270° and throughout the upstroke of the airfoil motion, the boundary layer is attached and laminar.

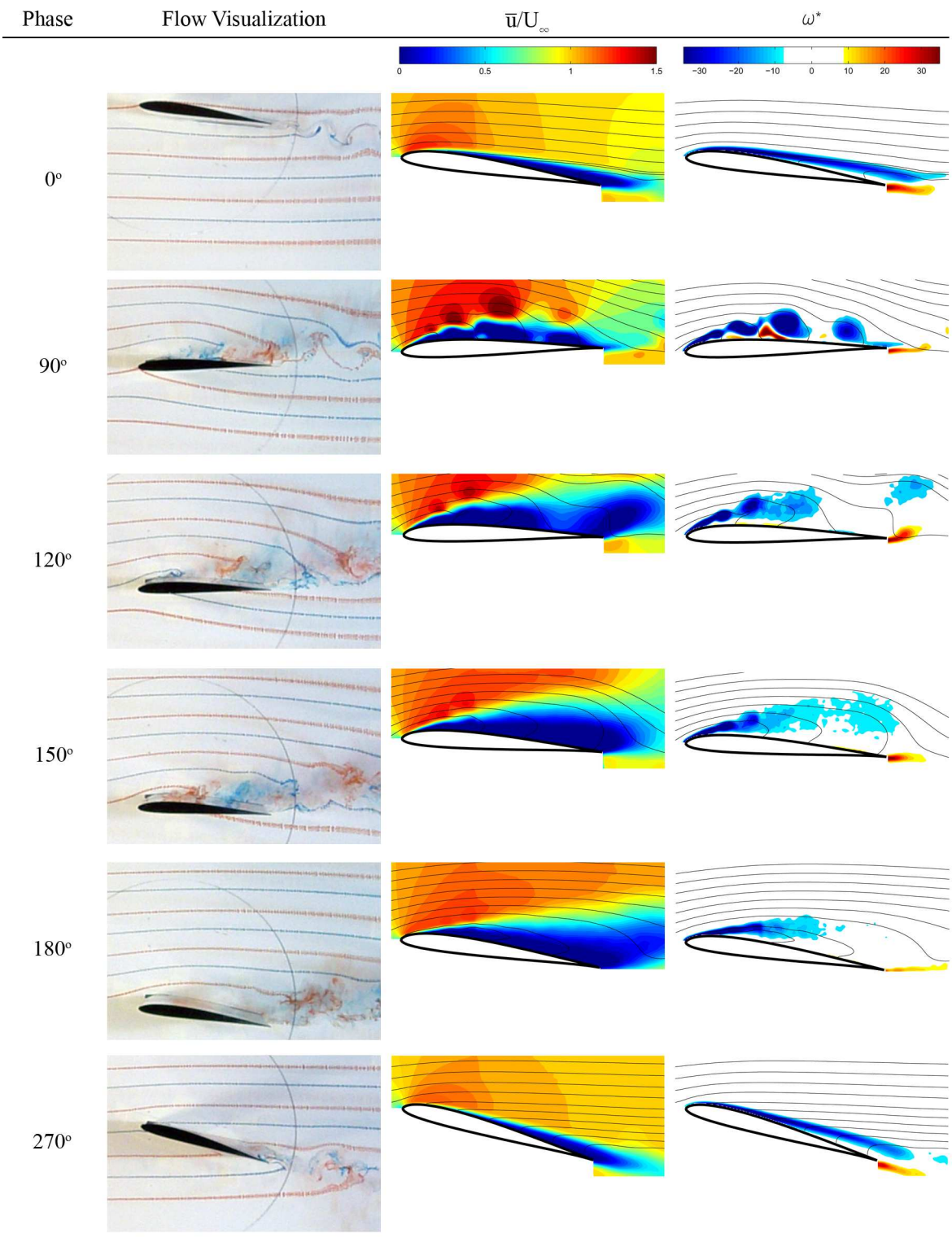

Figure 4. Flow visualization and PIV result for pitching and plunging SD7003 at $Re = 10,000$

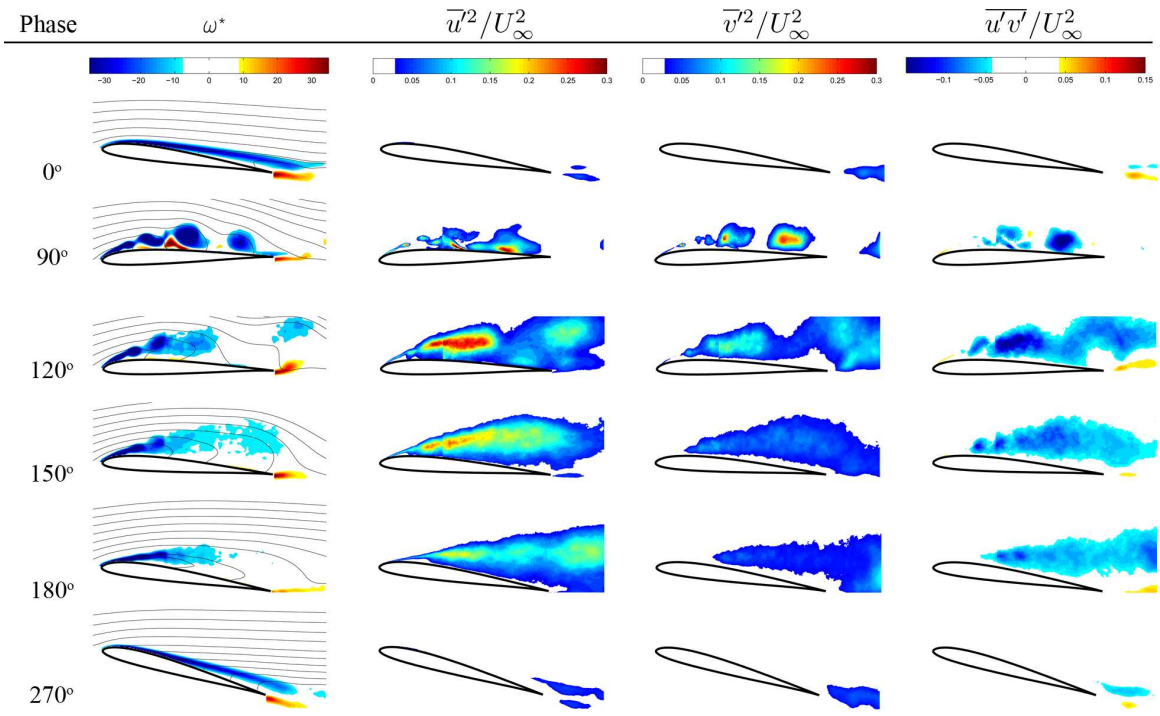

Figure 5. Turbulence statistics for pitching and plunging SD7003 at $Re = 10,000$

Figure 6 shows side-by-side comparison of UM dye flow visualization, PIV phase-averaged velocity field data and PIV phase-averaged vorticity field data for the pitching and plunging SD7003 at Re = 60,000. Figure 7 shows PIV phase-averaged vorticity field and the phase-averaged turbulence statistics (normalized $\overline{u'^2}$, $\overline{v'^2}$ and $\overline{u'v'}$ correlations). As in other cases there is excellent correlation between the flow visualization results and the flow field data. At phase 0° the boundary layer flow is attached and shows some transitional vortical structures past $x/c \approx 0.5$ and in the near wake. As in the lower Re case the transitional flow features are synchronized with the airfoil motion and persist through the phase averaging process. The $\overline{u'^2}$ and $\overline{v'^2}$ correlations are large at the center of the disturbances, while the $\overline{u'v'}$ remains relatively small in those regions. These results could be associated with large cycle-to-cycle variations of the location of the transitional features and a lack of three-dimensional smaller scale turbulent structures. At phases 90° through 180° the boundary layer is attached and turbulent. Transition occurs relatively close to the leading edge and, although some transitional features are observed at some phases, the $\overline{u'v'}$ correlation are relatively large and confined to the attached turbulent boundary layer. At phase 270° the flow field is very similar to phase 0° showing attached flow and transitional flow features near $x/c \approx 0.5$. These measurements were also conducted at Re = 30,000 which showed a flow topology very similar to the Re = 60,000 case. For completeness the Re = 30,000 results are shown in the Appendix and are not discussed here.

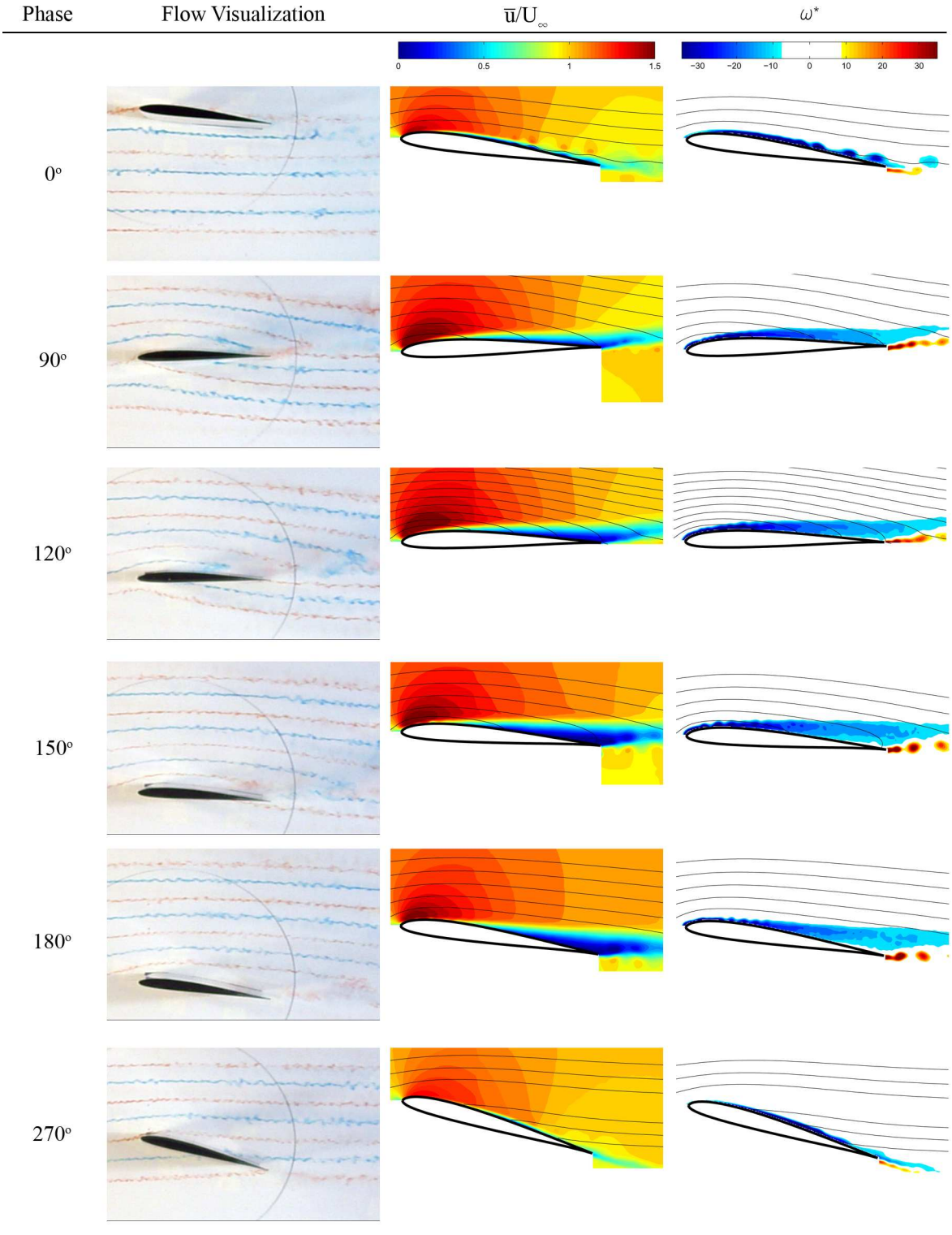

Figure 6. Flow visualization and PIV result for pitching and plunging SD7003 at $Re = 60,000$

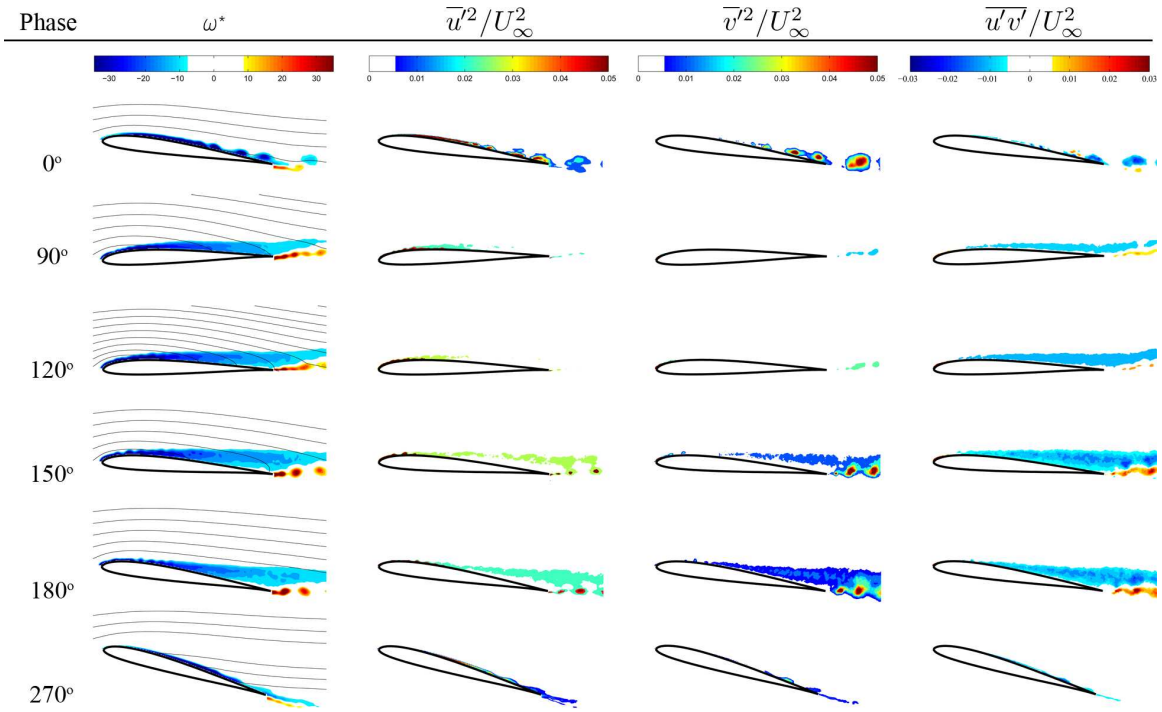

Figure 7. Turbulence statistics for pitching and plunging SD7003 at $Re = 60,000$

B. SD7003: Pure plunging motion

The fluid dynamic response to the pure plunging motion shows formation of leading edge and trailing edge vortices on both flow visualization and PIV flow field data. Figure 8 shows side-by-side comparison of UM dye flow visualization, PIV phase-averaged velocity field data and PIV phase-averaged vorticity field data for the pure plunging SD7003 airfoil at Re = 60,000. Figure 9 shows PIV phase-averaged vorticity field and the phase-averaged turbulence statistics (normalized $\overline{u'^2}$, $\overline{v'^2}$ and $\overline{u'v'}$ correlations). The correlation between the flow visualization results and the flow field data is excellent. At phase 0° the boundary layer flow is attached; there is no evidence of transitional vortical structures observed in the pitching plunging case at the same phase. At phases 90° through 180° the boundary layer separates near the leading edge and forms a large Leading Edge Vortex (LEV). A separated shear layer at the leading edge feeds vorticity to the LEV from phases 90° to 120°. The phase-averaged turbulence statistics show large $\overline{u'^2}$ and $\overline{v'^2}$ thoughout the entire LEV structure. The $\overline{u'v'}$ correlation is negative in the LEV vortex and positive in the shear layer feeding the LEV, which suggest that two fundamentally different processes are at work. Within the LEV vortex core the $\overline{u'v'}$ correlation is produced by small scale three dimensional turbulent structures. The strong mixing shown by the flow visualization images in the LEV vortex core is another manifestation of the smaller scale turbulent structure. As in other cases significant anisotropy is found in the turbulent fluctuations with $\overline{u'^2}$ fluctuation amplitude much larger than the $\overline{v'^2}$ fluctuation amplitude. At phase 150° the LEV moves downstream and the shear layer at the leading edge is not as well defined. A Trailing Edge Vortex (TEV) with positive (counterclockwise) vorticity is shed from the pressure side of the airfoil. The TEV core is approximatley $0.1c$ and the 2nd order turbulence statistics show an isotropic correlation between $\overline{u'^2}$ and $\overline{v'^2}$. The $\overline{u'v'}$ correlation in the core of the TEV is negative in the upstream side of the core, and positive in downstream side. This $\overline{u'v'}$ core structure is attributed to the cycle-to-cycle motion of the TEV vortex core, but further investigation is necessary for clarification. The flow at phase 180° is similar to phase 150° except for the more diffused (larger diameter) TEV vortex core; but the same structure of the 2nd order statistics is observed. At phase 270° the flow field is very similar to phase 0 showing attached laminar flow. Again the transitional flow features observed in the pitching plunging case at the same Re are not found for the pure plunging kinematics. There is evidence of transitional vortical flow features in the near wake of the airfoil at phases 0° and 270°.

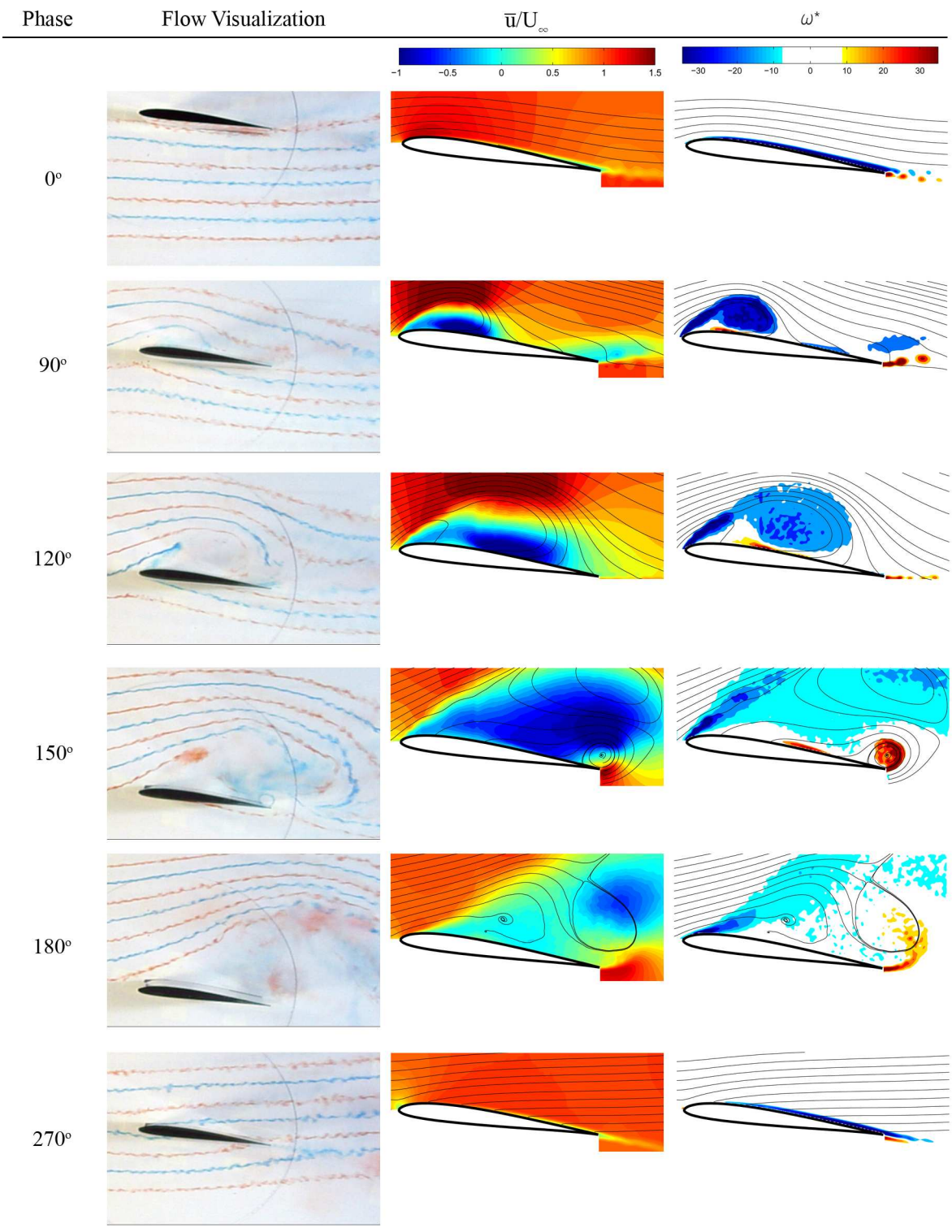

Figure 8. Flow visualization and PIV result for pure plunging SD7003 at $Re = 60,000$

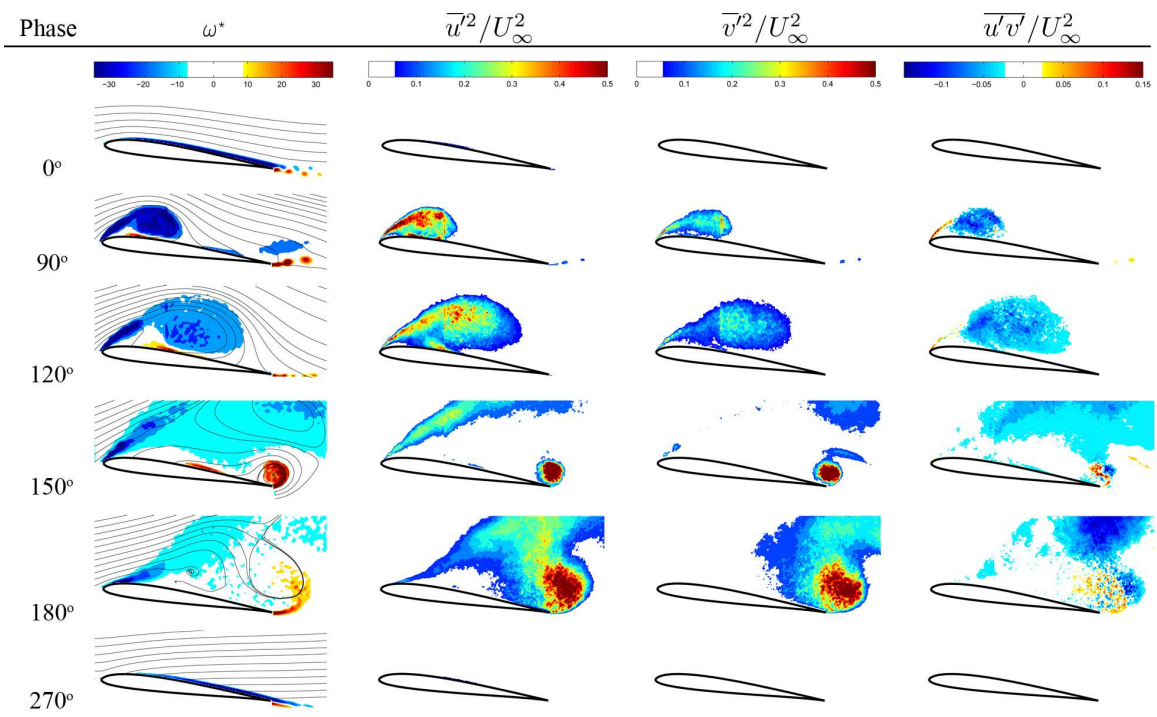

Figure 9. Turbulence statistics for pure plunging SD7003 at $Re = 60,000$

C. Flat Plate: Pitching and plunging motion

The flat plate model undergoing pitching and plunging motion at three different Re showed small Re effects, and only results for Re = 60,000 are discussed here. The results at other Re number are included in the Appendix. Figure 10 displays the flow visualization and PIV phase-averaged flow field measurements results, and Figure 11 plots the 2nd order phase-averaged turbulence statistics. The flow evolution in this case is somewhat different than for the SD7003 with the same kinematics and Re. At phase 0° the boundary layer flow is attached and shows transitional vortical structures near the leading edge and fully turbulent farther downstream along the chord. At phases 90° and 120° the flow separates near the leading edge and forms a closed separation region. The vorticity field in this case shows a relatively shallow vortical region compared to the LEV found in the pure plunging case for the SD7003 airfoil. The 2nd order velocity correlations show similar features of anisotropy in $\overline{u'^2}$ and $\overline{v'^2}$. At phases 150° and 180° the close recirculation region opens at the trailing edge and turbulent fluctuations are found in the bounding shear layer of the separated flow region. At phase 270° the fow field is very similar to phase 0° showing attached flow, transitional flow features near the leading edge and a turbulent boundary layer farther downstream along the chord.

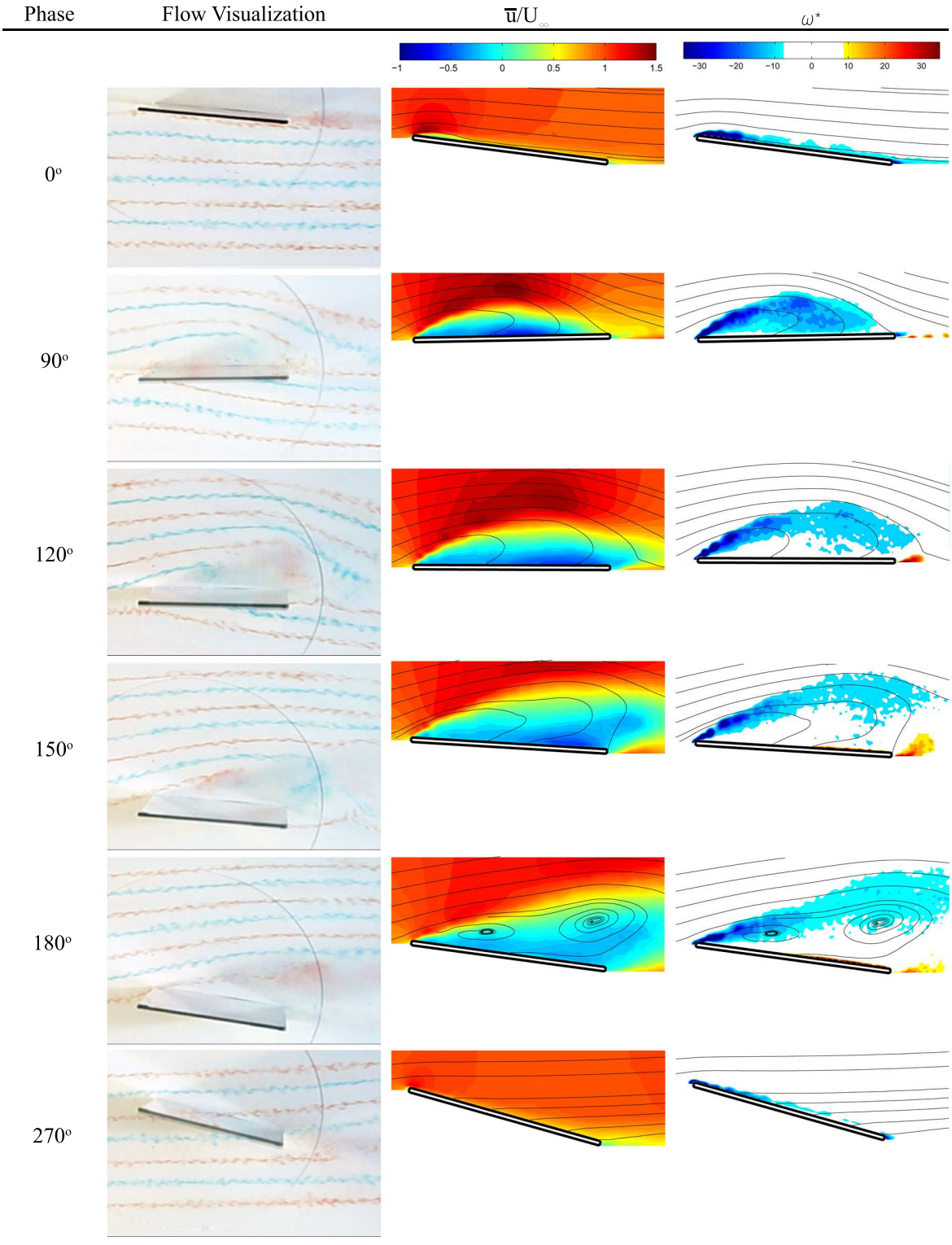

Figure 10. Flow visualization and PIV result for pitching and plunging flat plate at $Re = 60,000$

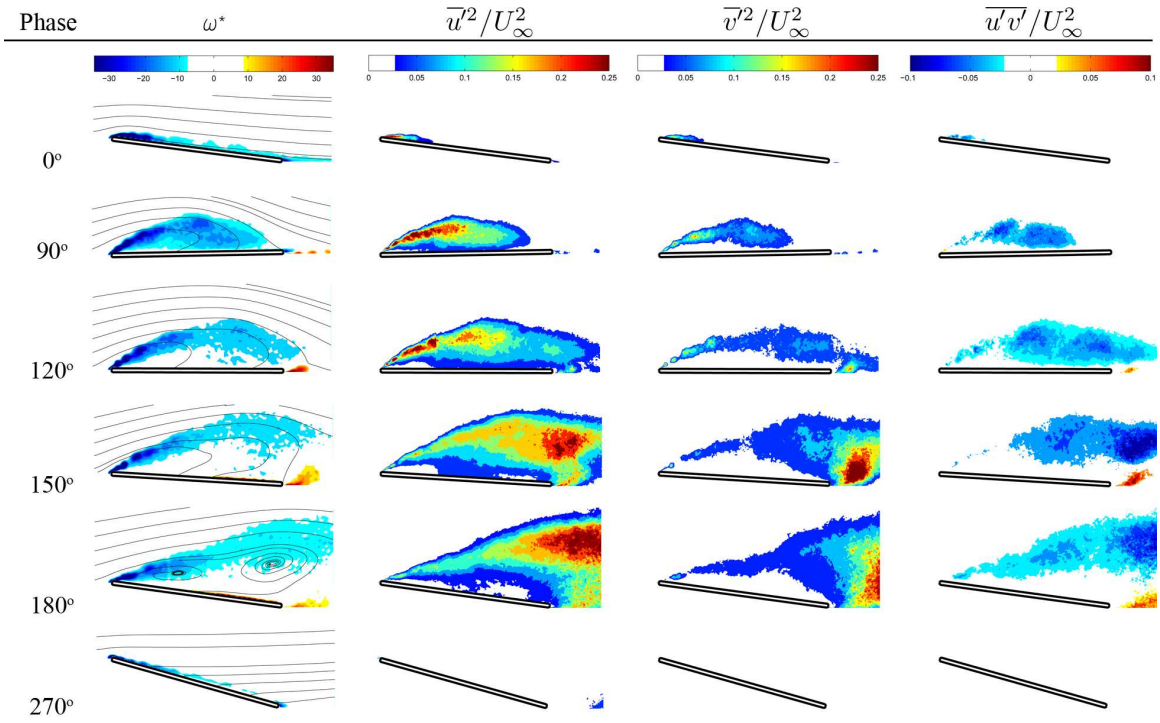

Figure 11. Turbulence statistics for pitching and plunging flat plate at $Re = 60,000$

D. Flat Plate: Pure plunging motion

The flow field for a pure plunging flat plate is similar to the SD7003 case for the same kinematics and Re. It encompasses the formation, development and detachment of the leading edge vortex followed by the introduction of a trailing edge vortex. Figures 12 and 13 summarize the flow visualization results, PIV phase-averaged flow field data and phase-averaged turbulence statistics for the flat plate undergoing pure plunging motion. The flow fields at phases 0° and 270° show the same features as for the flat plate in pitching plunging motion, namely attached flow with transitional vortical structures near the leading edge of the flat plate. The leading edge vortex is observed at phases 90° and 120°, and the trailing edge vortex is observed at phases 120° and 150°. The 2nd order statistics fields are very similar in structure compared to other cases showing the similar LEV and TEV vortical structures. Anisotrpy of $\overline{u'^2}$ and $\overline{v'^2}$ correlation fields; and $\overline{u'v'}$ correlation fields consistent with smaller scale turbulent structures and strong mixing. Phase 180° is somewhat unique in that there is no well defined vortex; only a thin detached shear layer at the leading edge. Although PIV data does not capture the wake region entirely, it can be estimated from the flow visualization that the size of the wake caused by the plunging motion is approximately the length of the chord. There are two noticeable differences between pure plunging of the SD7003 and flat plate. Firstly, the size and strength of the TEV of the flat plate is not as strong as in the SD7003 and it appears and dissipates earlier in the cycle (flat plate phase 120° –150° compared to SD 7003 phase 150° –180°). The turbulence statistics on the trailing edge vortex core shows similar $\overline{u'v'}$ structure with opposite sign values within the core that is similar to SD7003. Again, a possible jitter in the location of the trailing edge vortex may have caused this phenomenon. Secondly, the flow at phase 180° reattaches upstream of the trailing edge which creates an enclosed reverse flow region above the airfoil. The vorticity and turbulence correlation near the trailing edge are low while they are high at the leading edge.

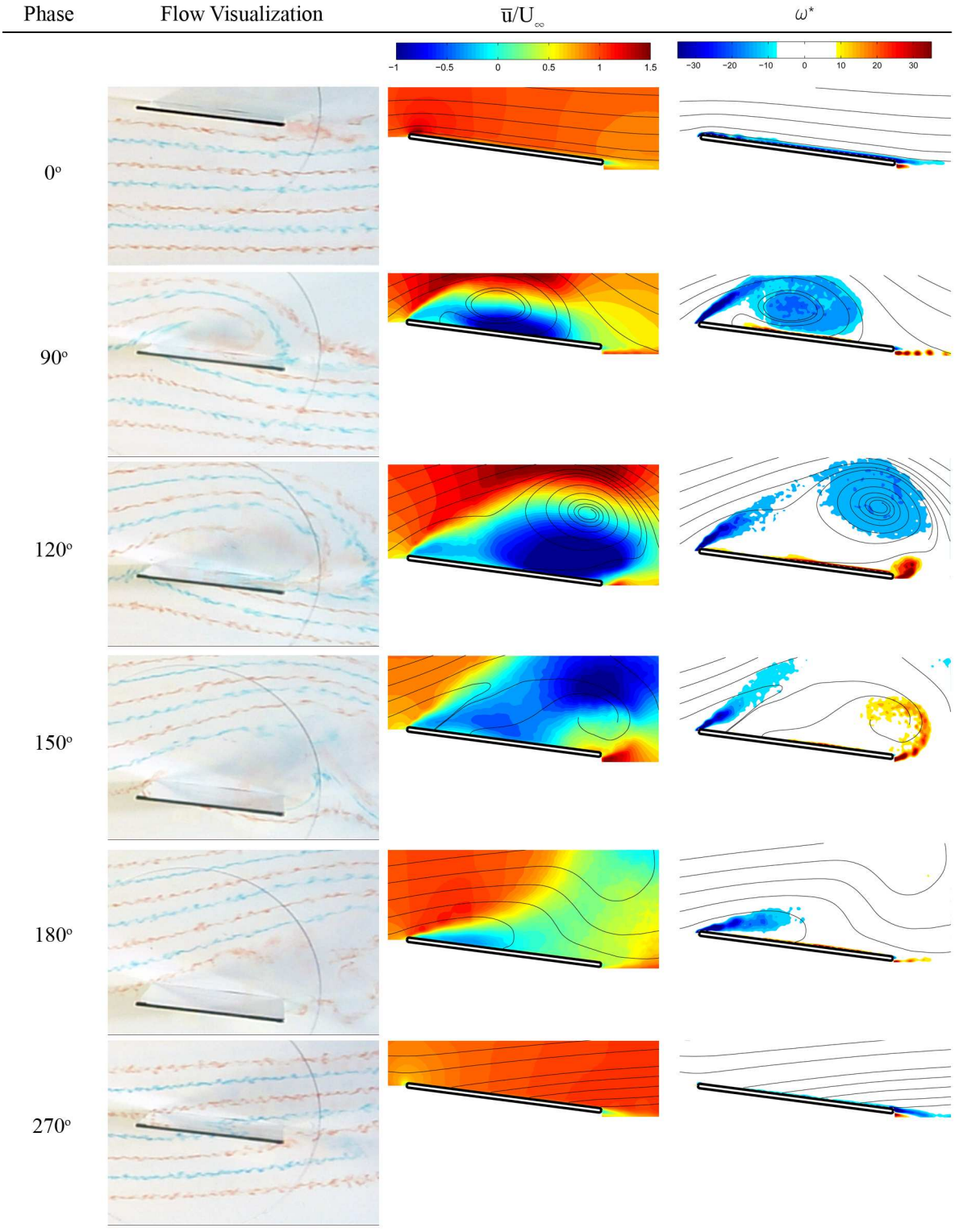

Figure 12. Flow visualization and PIV result for pure plunging flat plate at $Re = 60,000$

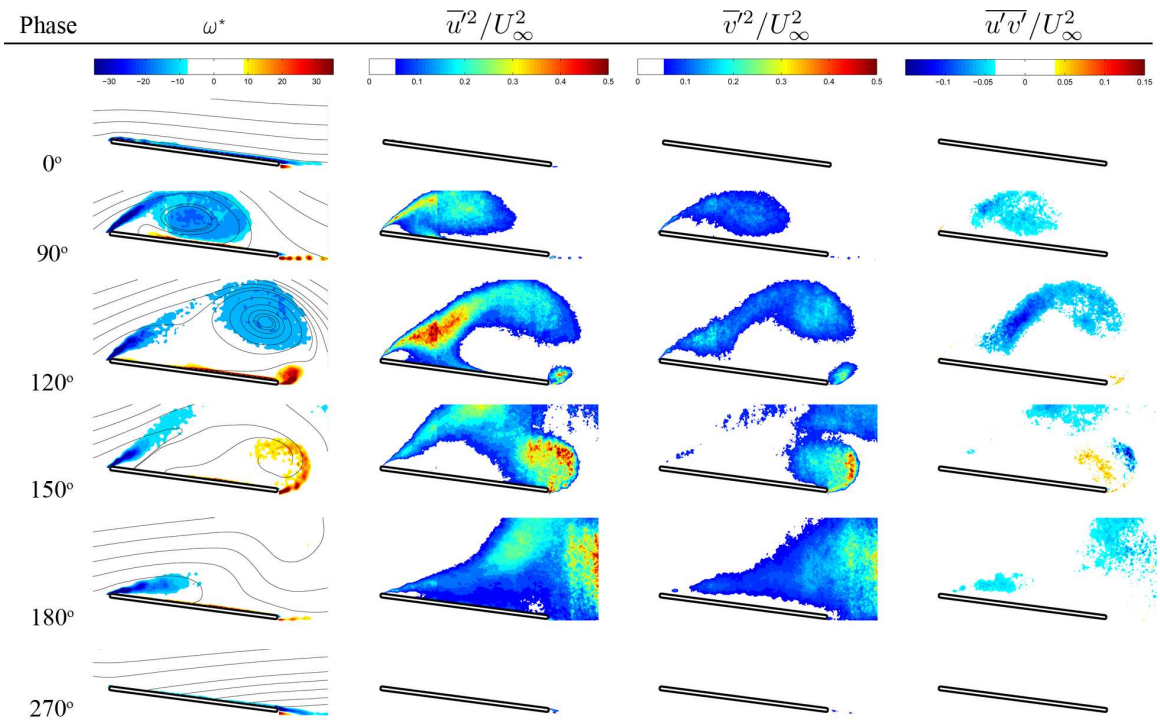

Figure 13. Turbulence statistics for pure plunging flat plate at $Re = 60,000$

E. Flow comparison between Univeristy of Michigan and AFRL

Figures 14 and 15 display flow visualization and PIV results obtained from both facilities for the pitching and plunging flat plate at Re = 60,000. The qualitative agreement in flow visualization is excellent; a relatively attached flow for SD7003, and leading edge separation characteristic for flat plate was observed at both facilities. While the flow visualization indicated similar flow properties for the pitching and plunging motion, a notable discrepancy was present in the PIV data sets. The major discrepancy was at phase 90° where UM PIV displayed enclosed reverse flow region above the chord but the AFRL data did not. This observation is clearly highlighted by the normalized vorticity contours.

The pure plunging case between the 2 facilities was also documented. The flow visualization presented in Figure 16 shows no notable discrepancies between the 2 facilities for both SD7003 and flat plate. However, PIV data comparison on pure plunging SD7003 airfoil reports strong disagreement in flow field near the end of the downstroke motion (Figure 17). At phase 90° and 120°, the formation and development of the leading edge vortex is captured in both facilities with the AFRL data showing slightly larger size of the vortex. The qualitative agreement of PIV data between 2 facilities is acceptable at these phases. The disagreement in the flow field becomes distinctive as the comparison continues to subsequent phases, namely phase 150° and 180°. At phase 150°, UM PIV data indicates a large and strong reverse flow above the trailing edge due to the formation of a strong trailing edge vortex. On the other hand, the formation of weaker trailing edge vortex does not induce as strong of a reverse flow region in AFRL PIV data. At phase 180°, the flow is mostly attached for the AFRL data while the flow still remains largely separated in UM data.

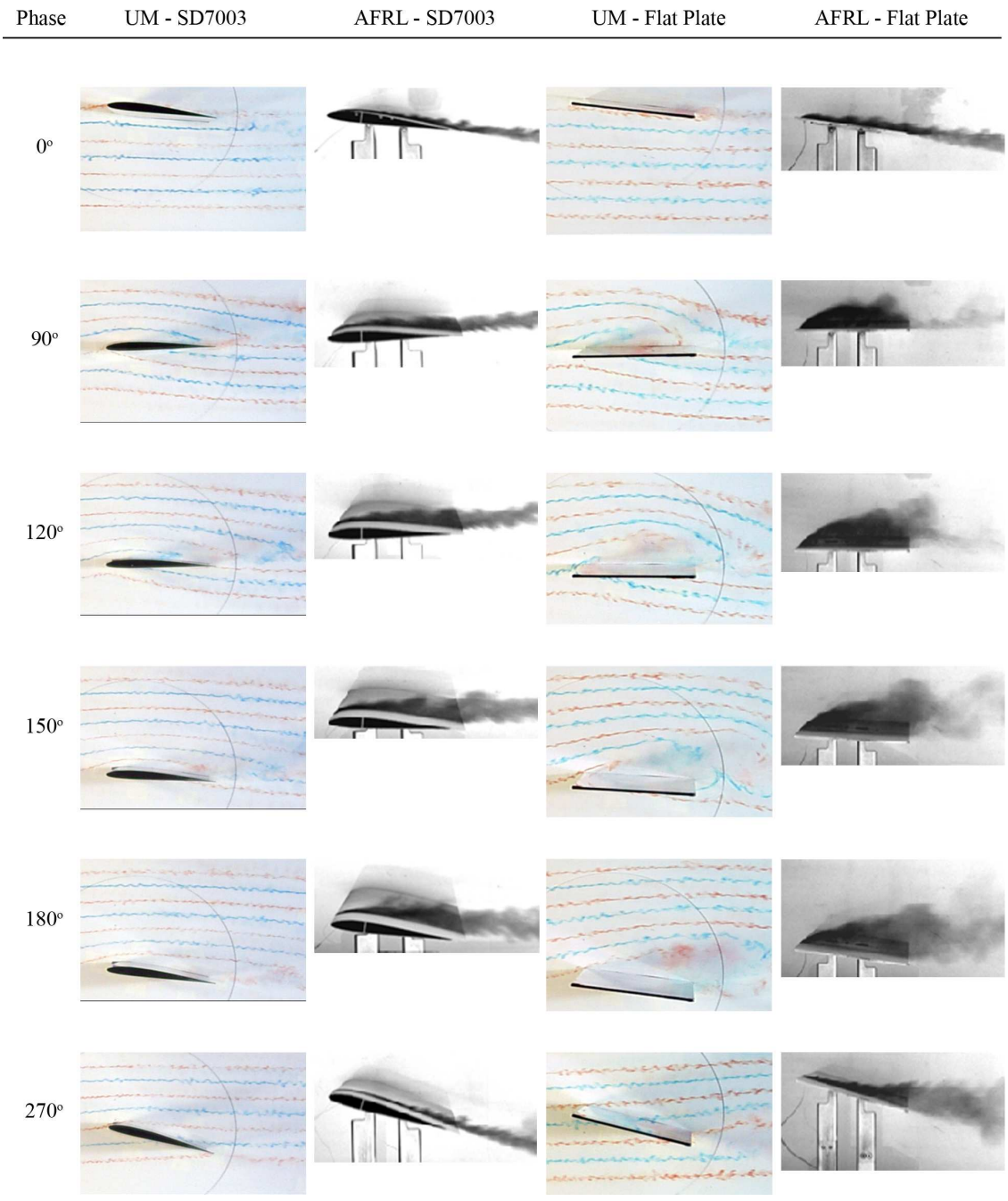

Figure 14. Flow visualization for pitching and plunging SD7003 (LEFT) and flat plate (RIGHT) at Re = 60,000

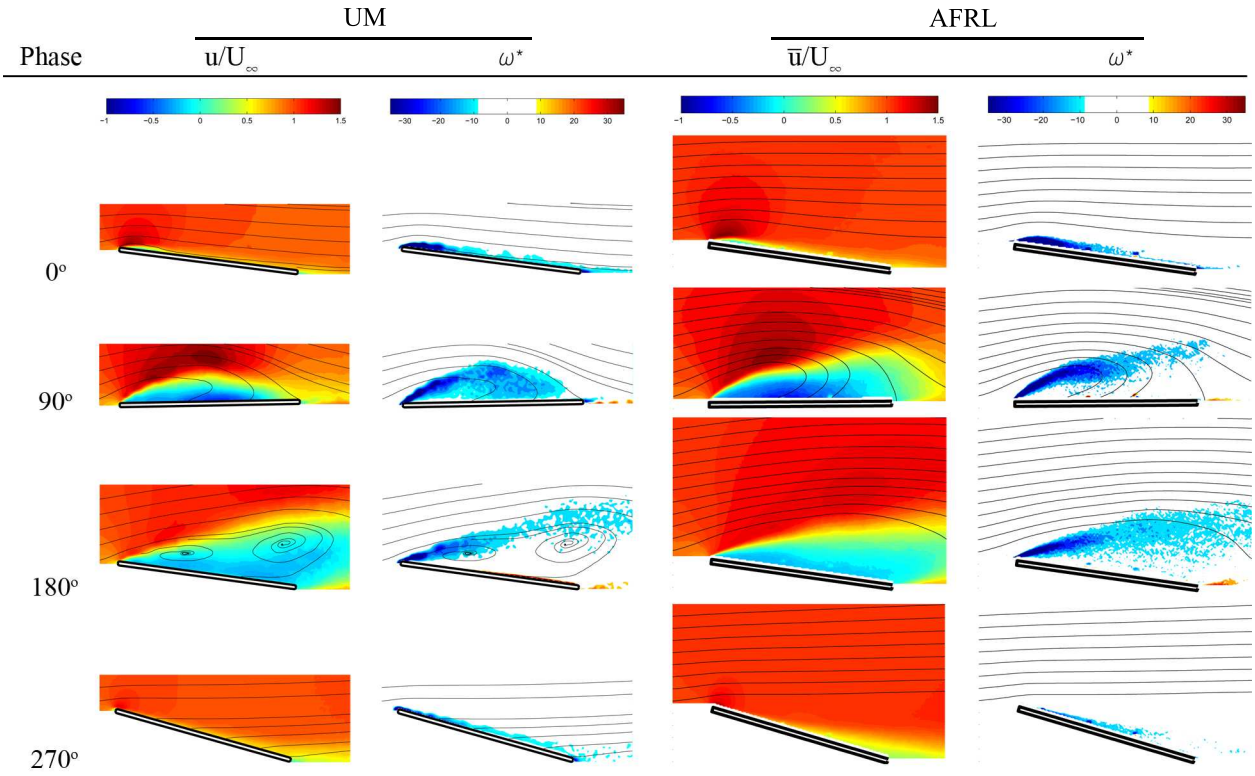

Figure 15. PIV data for pitching and plunging flat plate: University of Michigan (LEFT) and AFRL (RIGHT)

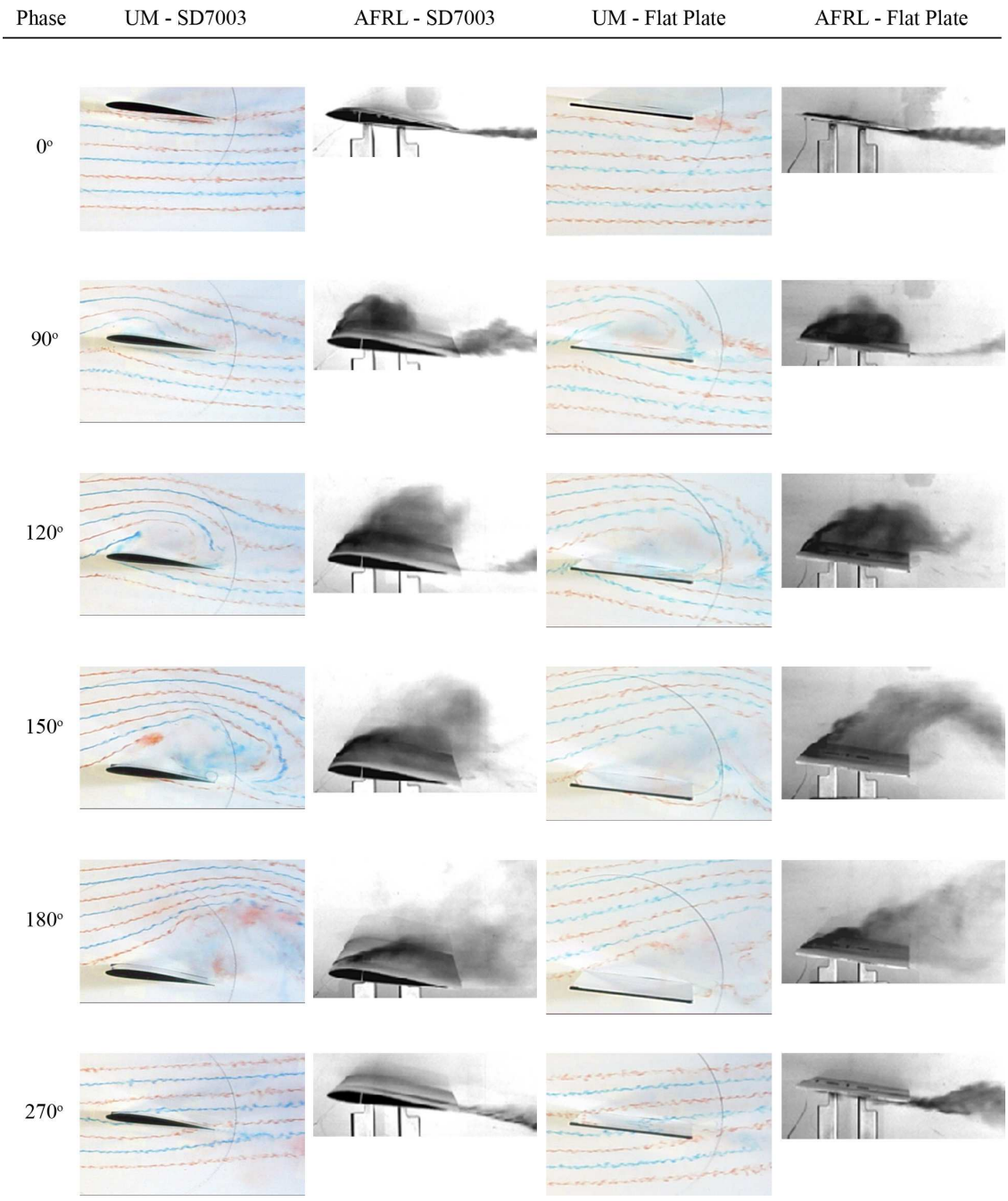

Figure 16. Flow visualization for pure plunging SD7003 (LEFT) and flat plate (RIGHT)

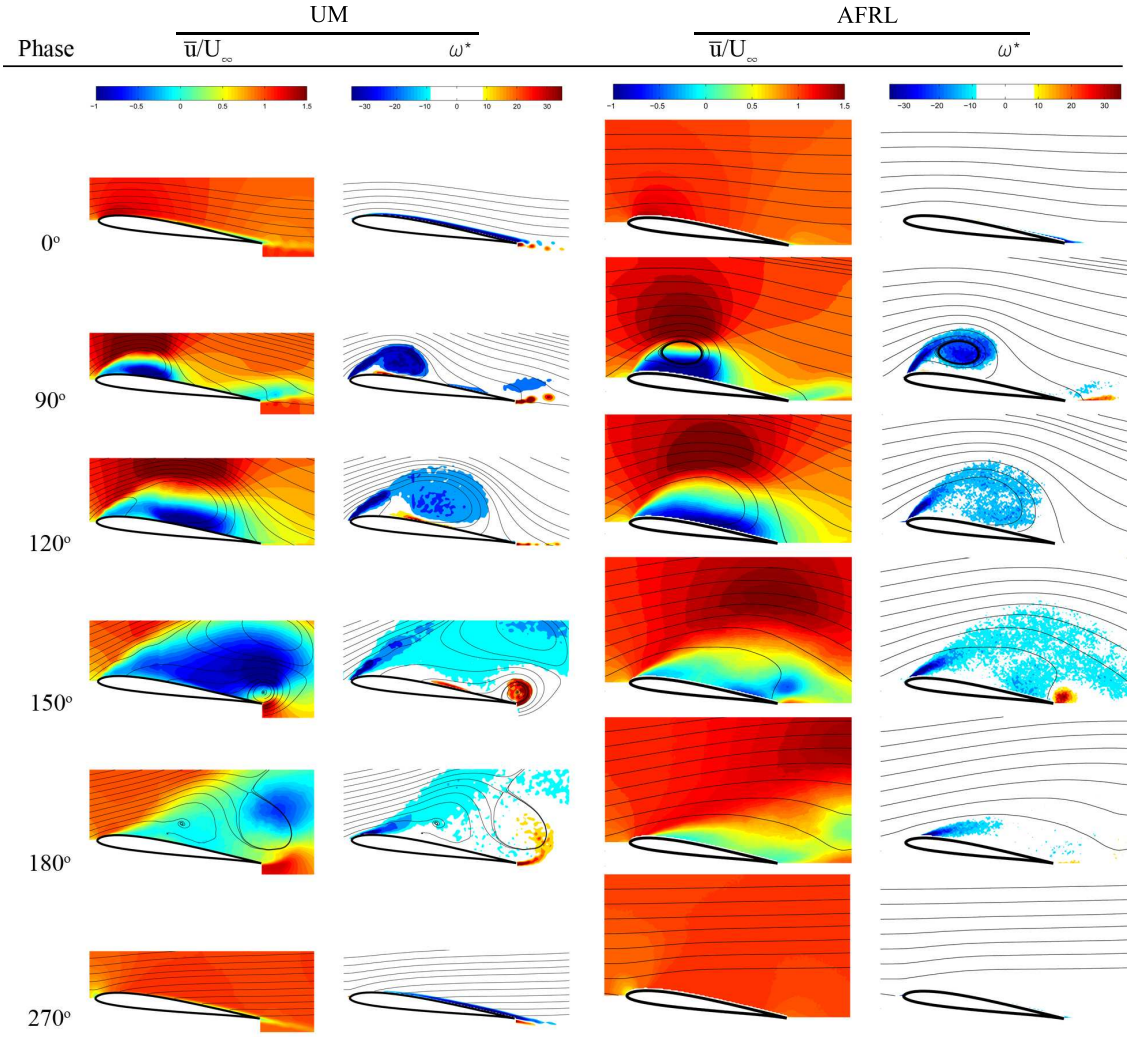

Figure 17. PIV data for pure plunging SD7003: University of Michigan (LEFT) and AFRL (RIGHT)

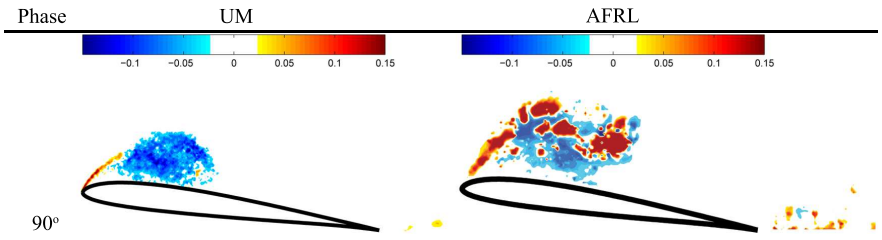

Figure 18. Turbulence statistics for pure plunging SD7003 at $Re = 60,000$

The agreement in PIV data between UM and AFRL for pure plunging case was adequate at phase 90°. Figure 18 compares the $\overline{u'v'}$ contours obtained from both facilities. The overall qualitative features are in good agreement but there exists a large discrepancy with the sign and magnitude of $\overline{u'v'}$ inside the leading edge vortex. There are numerous explanations to why there exists such discrepancy but the lack of convergence in 2nd order statistics might be the leading reason. Pure plunging motion introduces unsteady and high shear regions where more than 200 ensemble averaging might be required for 2nd order statistics convergence.

IV. Discussions

A. *Re* effect on SD7003 and flat plate

The *Re* effect found on pitching and plunging SD7003 was characterized by the laminar to turbulent transition and flow separation. At Re = 30,000 and 60,000, the flow remained relatively attached due to development of turbulent boundary layer near the leading edge. At Re = 10,000, laminar flow was reported at phase 0° and 270°, and laminar to turbulent transition occured during the downstroke motion.

The flow topology of the flat plate was predictable in a sense that the leading edge separation was expected due to sharp leading edge for the same motion experienced by SD7003. However, the characteristics of leading edge separation for different Re subjected to unsteady flow conditions was unforeseeable. The analysis from the velocity and vorticity contour plots qualitatively suggested a minimal Re effect. This observation was confirmed quantitatively by comparing velocity profiles along different chord locations at all phases. Figure 19 plots flat plate velocity profiles at selected chord locations for phase 90° and 180°.

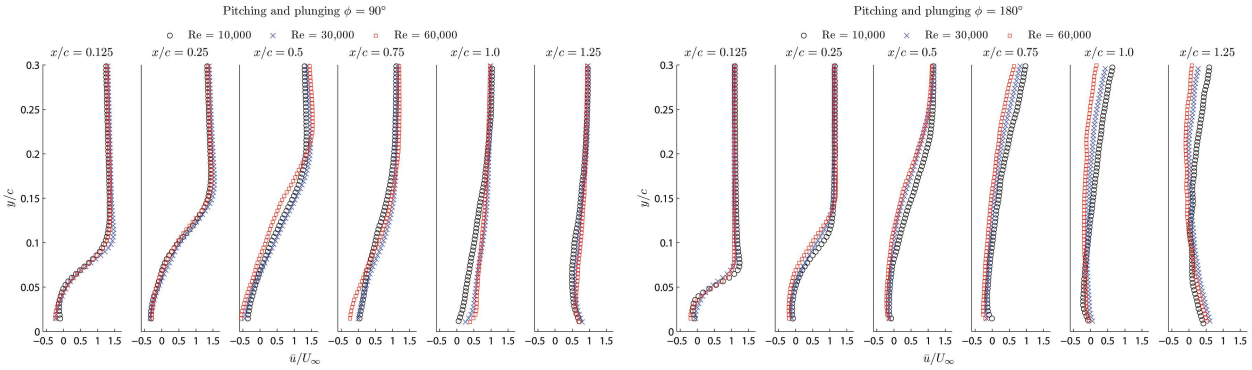

Figure 19. Phase 90° (LEFT) and phase 180° (RIGHT) flat plate velocity profiles at selected chord locations for Re = 10,000, 30,000 and 60,000

The comparison shows slight discrepancies on the slope and the magnitude of the velocity in the profiles at different chord locations, but there are no clear distinctive *Re* effect. Phase 180° contained a small trend in the flow structure where the seperation region thickened as Re was increased. To some extent, this was observed from the contour plots but the Re effect observed for the flat plate was minimal compared to that of SD7003.

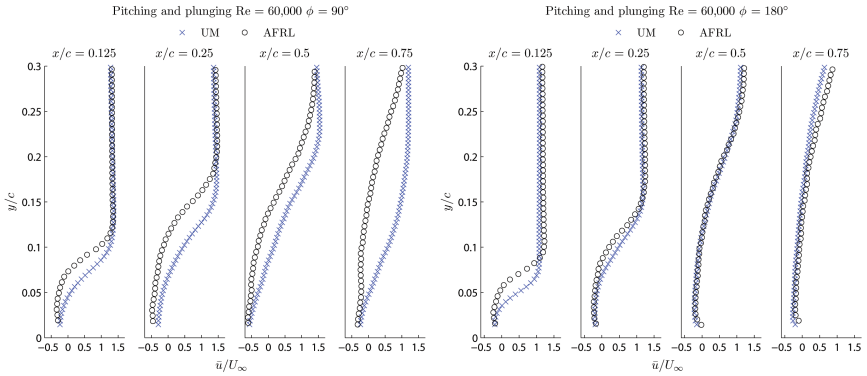

Figure 20. Comparison between UM and AFRL PIV data

A quantitative agreement of PIV results from UM and AFRL was acceptable. A strong discrepancy was observed at the midway of the downstroke of the motion. Figure 20 plots velocity profiles at phase 90° and 180° to illustrate the discrepancy. The main discrepancy was observed at phase 90° at $x/c = 0.75$ where the flow field remained largely separated for AFRL data. UM data showed reattachment of the flow which led to an enclosed reverse flow region. Despite the differences in the flow field at phase 90°, a reasonable agreement was made at phase 180°. The flow is fully separated from the leading edge at 180° and similarity

between AFRL and UM at this phase may indicate early separation characteristic in AFRL facility. Recall that phase 120° showed burst of the enclosed region which is analogous to the 90° of AFRL data. Since the AFRL data set at Re = 10,000 and 30,000 was unavailable, the implication of discrepancy was inconclusive; the discrepancy could imply the Re effect on the flat plate that exists in AFRL facility, or it could simply be the difference in experimental conditions that alter the fluid dynamic responses to the pitching and plunging motion of the flat plate.

B. Cross-section geometry effect on flow separation

The main difference between SD7003 and flat plate is the airfoil cross-section. SD7003 has approximately 8.5% thickness with slight camber, and flat plate has much lower thickness value of 2.3%. In order to assess the effect of airfoil cross-section, velocity profiles for SD7003 at Re = 10,000 and 60,000, and flat plate at Re = 10,000 were compared. The choice of flat plate velocity proflie at Re = 10,000 as a representative profile was arbitrary; for this comparison the velocity profiles for flat plate at all Re were assumed to be identical since it was found that Re effect was minimal for the flat plate. Figure 21 plots velocity profiles at selected chord locations for phase 0° and 90°.

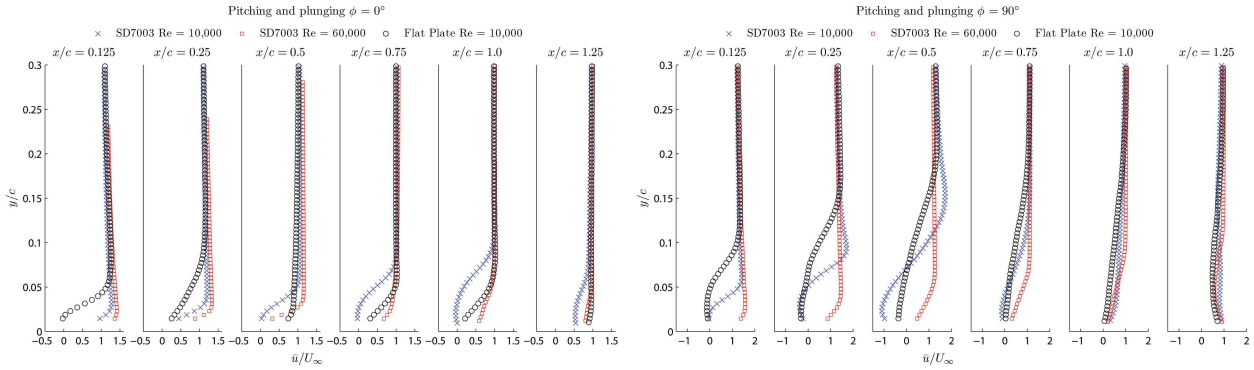

Figure 21. Velocity profiles at selected chord locations for SD7003 and flat plate at phase 0° (LEFT) and phase 90° (RIGHT)

Figure 21 depicts interesting features of the flow field around SD7003 and flat plate. At phase 0°, SD7003 at Re = 10,000 displays development of a boundary layer and small region of reverse flow is present at x/c = 0.75. At Re = 60,000, the flow remains fully attached at all chord locations. For the flat plate, turbulence statistics showed laminar separation at the leading edge and reattachment to a turbulent boundary layer between x/c = 0.25 and x/c = 0.5. The change in the velocity gradient along the chordwise direction clearly illustrates this phenomena. At phase 90°, the comparison between pitching and plunging SD7003 at Re = 60,000 and flat plate is trivial since the flow characteristic are completely different; SD7003 at Re = 60,000 has flow field that is relatively attached and flat plate does not. For SD7003 and flat plate at Re = 10,000, both models hinted an attached flow near the trailing edge which led to an enclosed reverse flow region above the chord.

An interesting observation can be made for Re = 10,000 SD7003 and flat plate at phase 180° (Figure 22). By shifting the velocity profile of SD7003 by x/c = 0.25 towards the leading edge, it would suggest an existence of a delay in the separation characteristic for SD7003. Figure 23 explores the possibility of delayed flow response on SD7003 by shifting the SD7003 velocity profile by x/c = 0.25 towards the leading edge at Re = 10,000.

It is evident from Figure 23 that SD7003 experiences delay in the flow development by approximately x/c = 0.25 at phase 150° and 180°. This implies the leading edge curvature effect where flat plate has a sharper leading edge that causes the flow to separate sooner. However, this delay was not found at earlier phases, namely phase 90° and 120°. A possible explanation for this observation would be the recirculating zone created at the leading edge; the delayed response is only seen when the recirculating zone no longer resides on top of the airfoil.

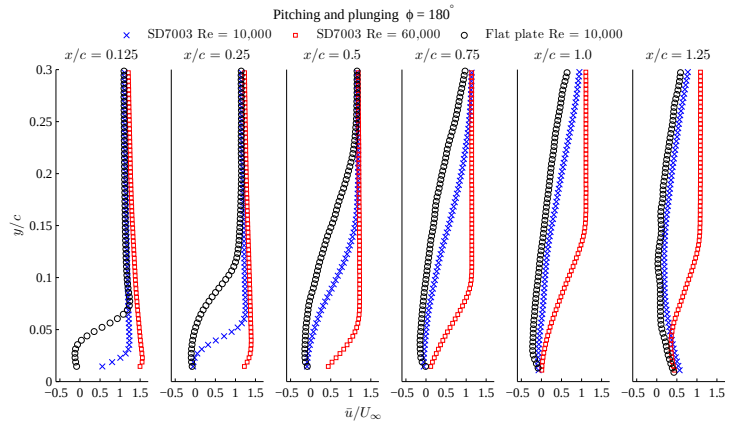

Figure 22. Velocity profiles at selected chord locations for SD7003 and flat plate at phase 180°

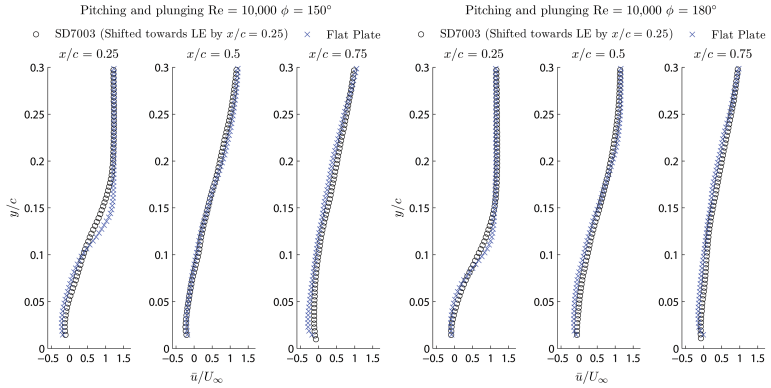

Figure 23. Phase 150° (LEFT) and 180° (RIGHT) velocity profiles comparison of SD7003 and flat plate at Re = 10,000 with SD7003 profiles shifted towards the leading edge by $x/c = 0.25$

C. Leading edge shape effect on the development of leading edge vortex

Pure plunging airfoil kinematics corresponds to more aggressive $\alpha_{\text{eff}}(t)$ as well as higher peak-to-peak $\alpha_{\min}$ and $\alpha_{\max}$ values. These changes are expected to enhance the leading edge flow separation characteristics on SD7003 where flow remained relatively attached for high Re in pitching and plunging case. The formation of a strong leading edge vortex was observed for both models and apparent phase lag of 30° between phase 0° and 180° can be deduced from the contour plots and flow visualizations shown in Figure 24.

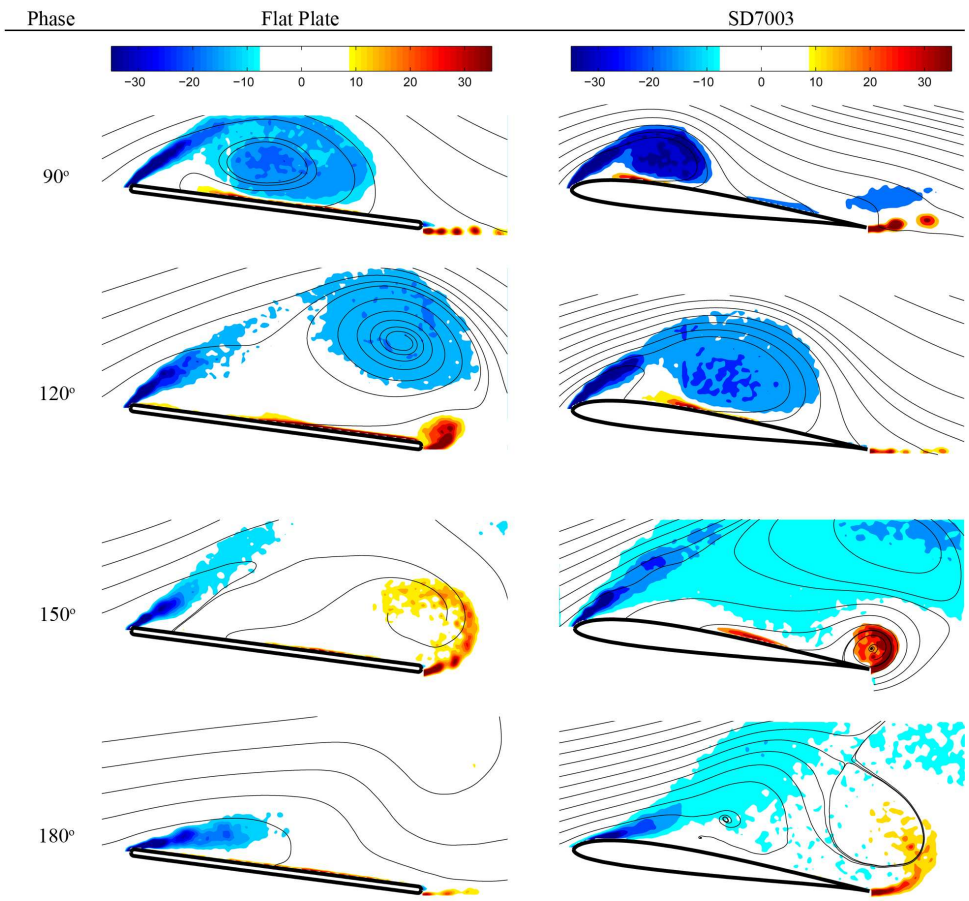

Figure 24. Comparison of normalized vorticity contour for flat plate and SD7003

In order to verify the phase lag of 30° in the flow field, velocity profiles of SD7003 obtained from UM and AFRL at various phases were shifted forward by 30° phase and were compared with the flat plate data. Figures 25 through 27 plots these velocity profiles. It is evident from Figure 25 that UM and AFRL SD7003 velocity profiles at phase 120° correlates well with the velocity profiles of flat plate at phase 90°. UM velocity profiles are in excellent agreement from $x/c = 0.5$ to $x/c = 1.25$ while AFRL velocity profiles showed better agreement between $x/c = 0.125$ and $x/c = 0.25$. A quantitative agreement between UM SD7003 and flat plate at phase 120° is excellent at $x/c = 0.25$ and $x/c = 0.5$ (Figure 26). A strong discrepancy at $x/c = 1.0$ is characterized by the strong positive velocity magnitude of SD7003 as it approaches the airfoil trailing edge. The trailing edge vortex is present at both phase 120° of flat plate and phase 150° of SD7003, but SD7003 possesses a sharp trailing edge whereas flat plate has the some curvature. The difference in trailing edge shape may contribute to a different trailing edge vortex size and strength, and therefore introducing the source of discrepancy. AFRL velocity profiles faired poorly against the flat plate data but this was to be expected given the qualitative discrepancies with UM PIV data observed from contour plots at phase 150°.

Figure 27 illustrates the diminishing effect of 30° phase lag as the motion nears the end of the downstroke motion. The velocity profiles at phase 150° for UM SD7003 compare better with flat plate from the leading edge to $x/c = 0.5$. On the other hand, UM SD7003 velocity profile at phase 180° is in a good agreement with flat plate between $x/c = 1.0$ and $x/c = 1.25$. This implies that the leading edge flow field around pure plunging flat plate at phase 150° resembles pure plunging SD7003 flow field at the same phase, but the near wake property resembles SD7003 at phase 180°. An interesting conclusion can be drawn from this observation by noticing the formation of the trailing edge vortex. The discrepancy in the initial size and strength of the trailing vortex led to a disagreement as shown in Figure 26. However, in a subsequent phase, Figure 27 suggests a quantitative agreement on the flow velocity when the trailing edge vortex has dissipated.

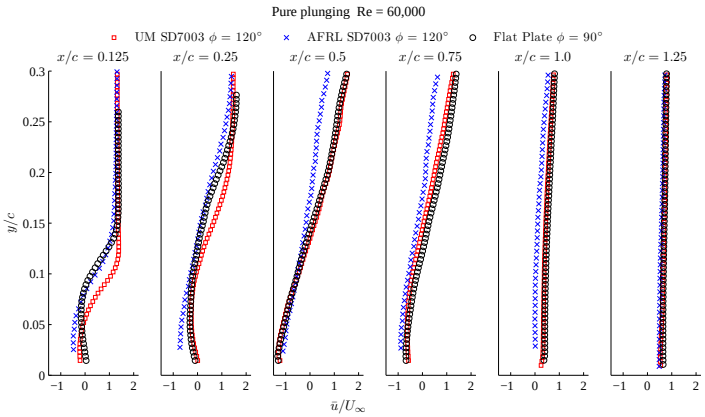

Figure 25. Pure plunging velocity profile of UM and AFRL SD7003 at phase 120°, and UM flat plate at phase 90°

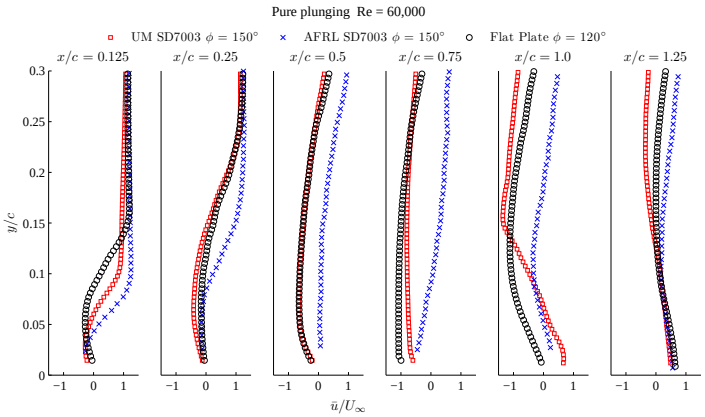

Figure 26. Pure plunging velocity profile of UM and AFRL SD7003 at phase 120°, and UM flat plate at phase 120°

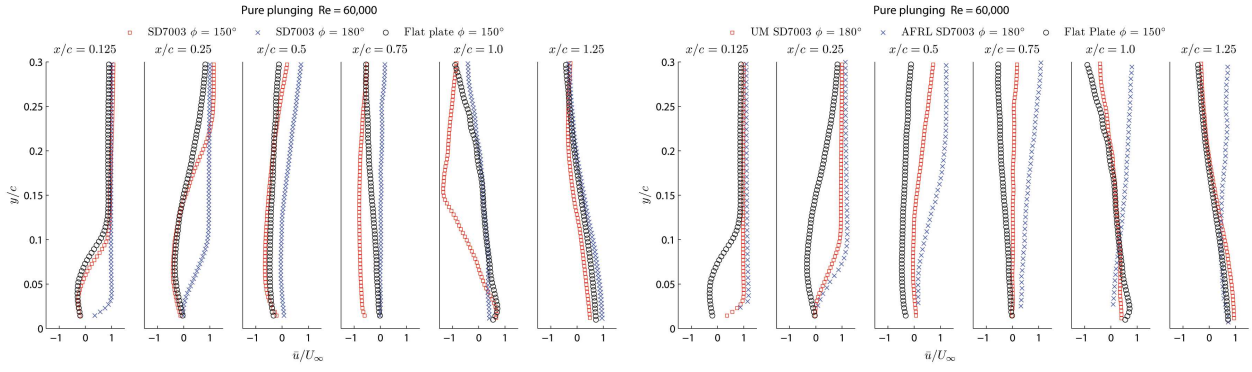

Figure 27. Pure plunging velocity profile of SD7003 and flat plate at phase 150°, and SD7003 at phase 180° (LEFT), velocity profile of UM and AFRL SD7003 at phase 180°, and flat plate at phase 150° (RIGHT)

V. Conclusions

An experimental study of SD7003 and flat plate model on a nominally 2D wing undergoing pitching and plunging motion was conducted. Phase-averaged 2D instantaneous flow field was captured for selected phases of the motion using PIV measurement technique at the University of Michigan and AFRL. Two sets of airfoil kinematics were used: a combined pitching and plunging at Re = 10,000, 30,000, and 60,000, and a pure plunging motion at Re = 60,000. Notable conclusions from current study include:

- Re effect was observed for pitching and plunging SD7003. At Re = 10,000 laminar boundary layer and laminar to turbulent transition was observed. For higher Re a turbulent boundary layer was present for all phases with laminar to turbulent transition occuring near the leading edge of the airfoil. The flow field was more attached than Re = 10,000.

- Re effect was minimal for pitching and plunging flat plate. The flow field was qualitatively and quantitatively similar for all Re. The leading edge separation was observed with transitional flow features near the leading edge at phase 0° and 270°. Turbulence statistics showed a larger $\overline{u'^2}$ fluctuation magnitude compared to $\overline{v'^2}$ fluctuation magnitude which hinted anisotropic turbulence.

- For pitching and plunging motion, SD7003 displayed a delayed development of separated flow region by approximately $x/c = 0.25$ compared to the flat plate. This observation was only apparent at phases 150° and 180° where the recirculating zones created by the leading edge during the downstroke motion were vanished. The effect of leading edge shape explained the delayed seperation characteristics.

- Pure plunging SD7003 and flat plate displayed similar qualitative and quantitative flow field features. Both models captured the formation, development and detachment of the LEV followed by the introduction of a TEV during the downstroke motion. Turbulence statistics showed anisotropy in $\overline{u'^2}$ and $\overline{v'^2}$ correlation for the LEV while isotropy was present for TEV. A shear layer feeding the LEV was noted by a thin positive $\overline{u'v'}$ that is explained by a possible cycle-to-cycle variation in the position of the shear layer. The strength of the trailing edge vortex was stronger for SD7003 due to sharper trailing edge shape.

- A phase lag of approximately 30° was observed in pure plunging SD7003 compared to pure plunging flat plate. A quantitative analysis showed a good agreement in the phase shifted velocity profiles where the LEV is present. The phase lag diminished as the airfoil approached the end of the downstroke motion. The difference in the leading edge shape caused delayed formation and development of LEV during the downstroke motion.

- UM and AFRL PIV data showed excellent agreement for attached flow fields but a notable discrepancy was shown for a leading edge separated flows. The flow fields in AFRL data displayed larger separated region compared to UM data at the midway of the downstroke motion (phase 90°). Turbulence statistics were in qualitative agreement but the lack of 2nd order statistical convergence prevented any quantitative analysis.

Appendix

A. UM Flow Visualization and PIV Results

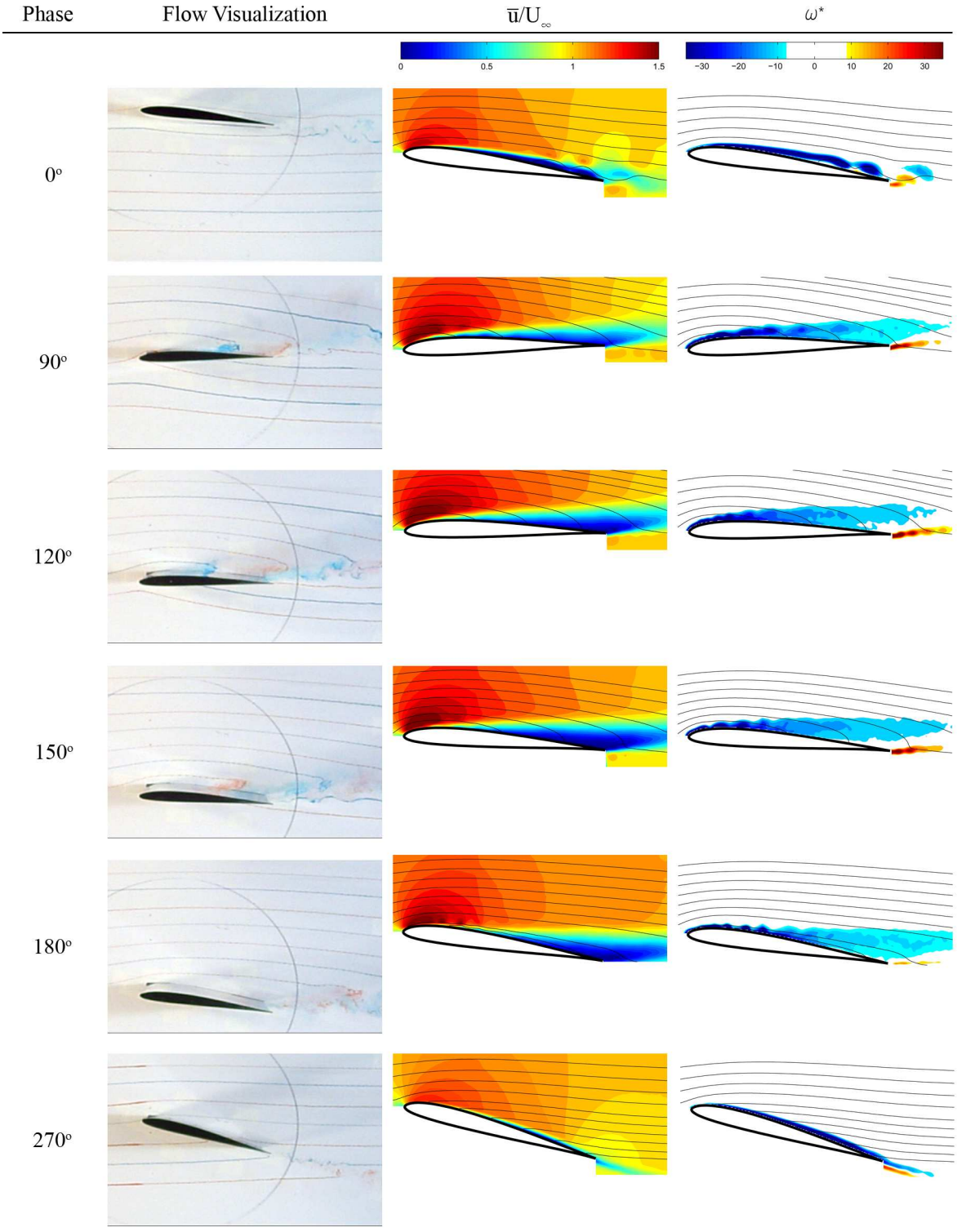

Figure A.1. Flow visualization and PIV result for pitching and plunging SD7003 at $Re = 30,000$

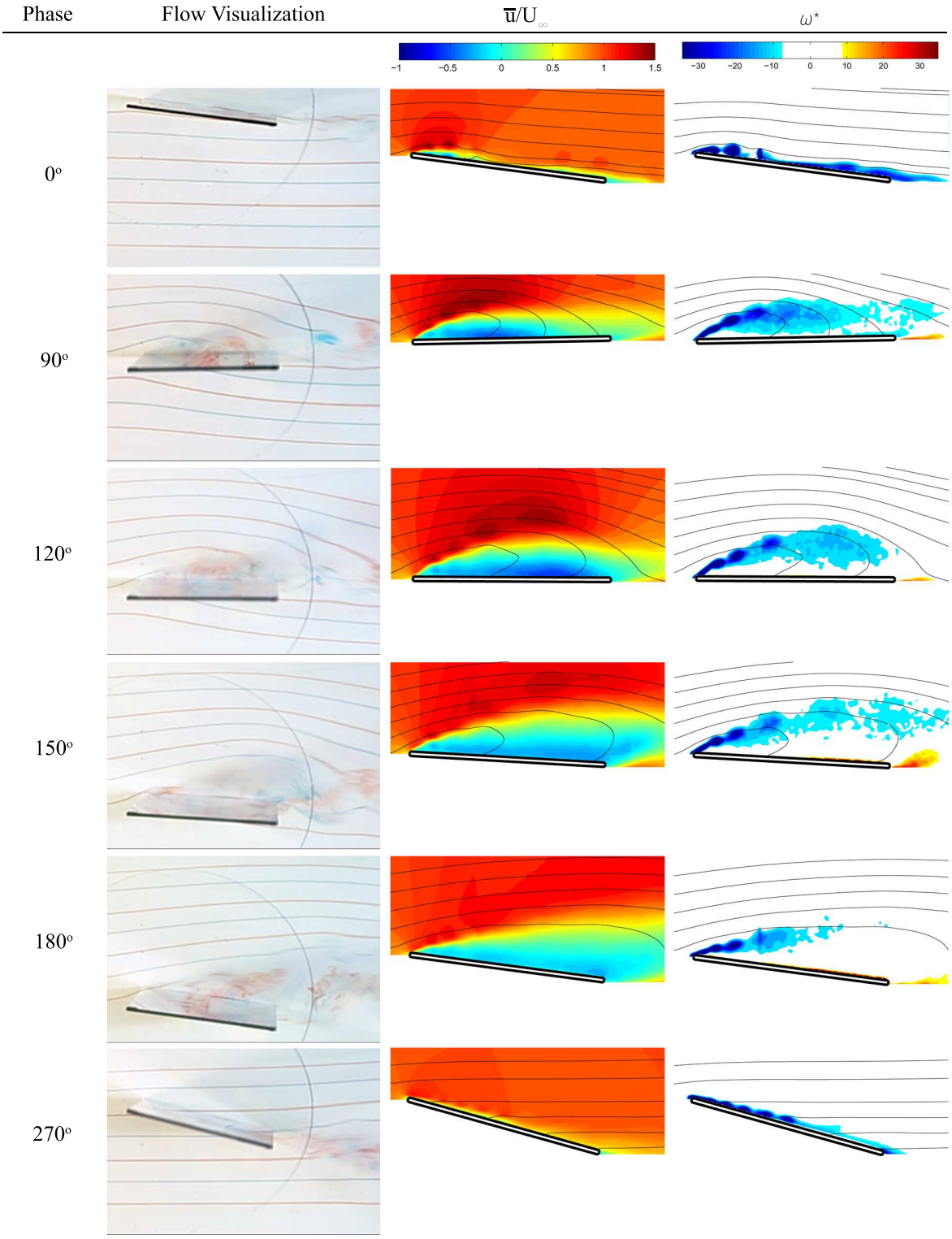

Figure A.2. Flow visualization and PIV result for pitching and plunging flat plate at $Re = 10,000$

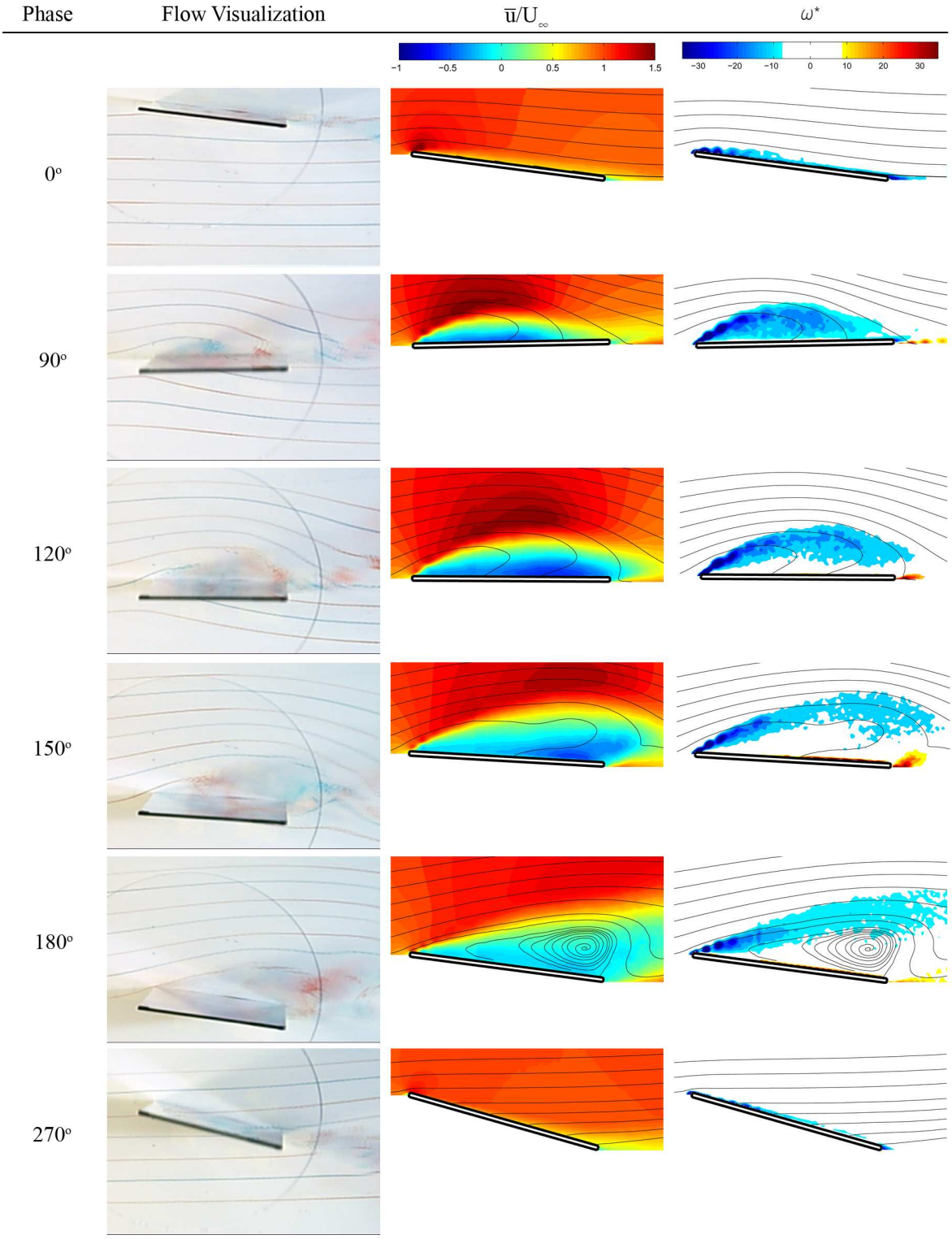

Figure A.3. Flow visualization and PIV result for pitching and plunging flat plate at $Re = 30,000$

B. UM PIV Data: 2nd Order Statistics

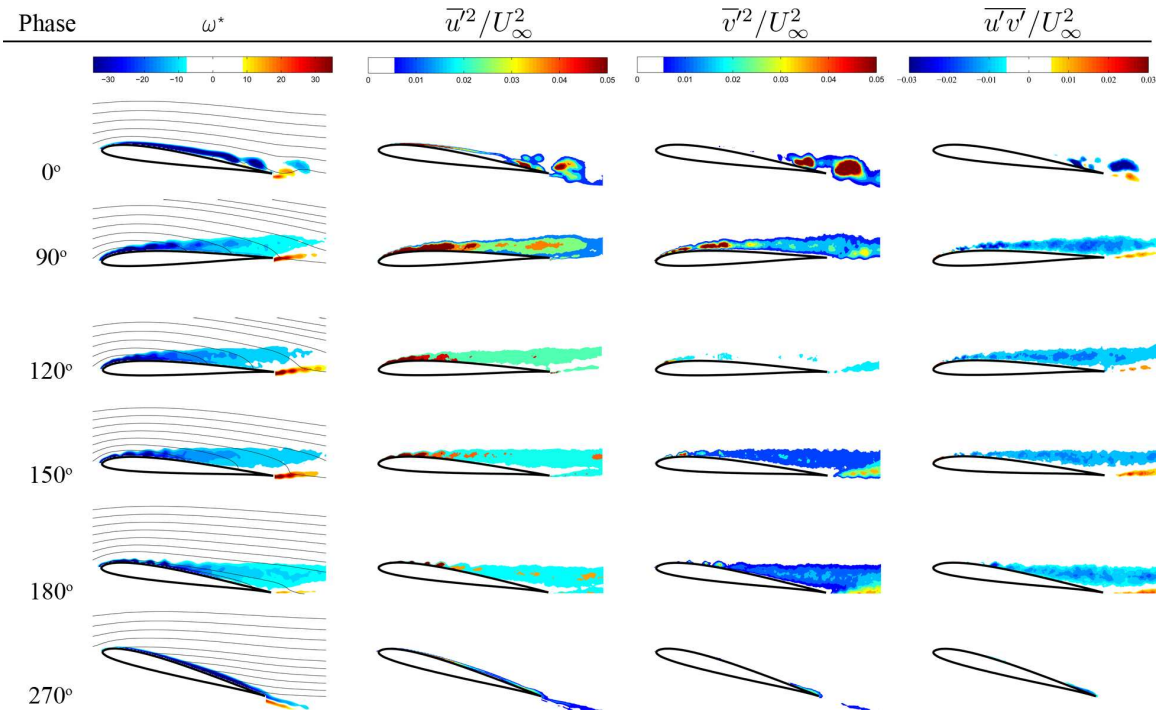

Figure B.1. Turbulence statistics for pitching and plunging SD7003 at $Re = 30,000$

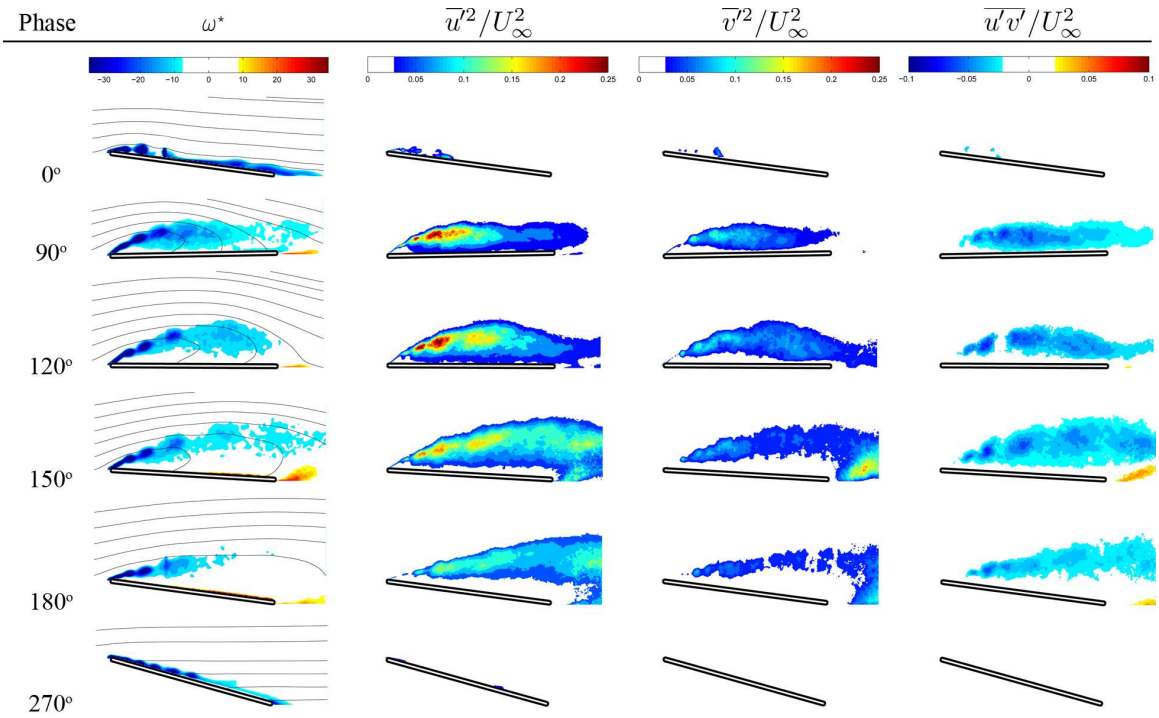

Figure B.2. Turbulence statistics for pitching and plunging flat plate at $Re = 10,000$

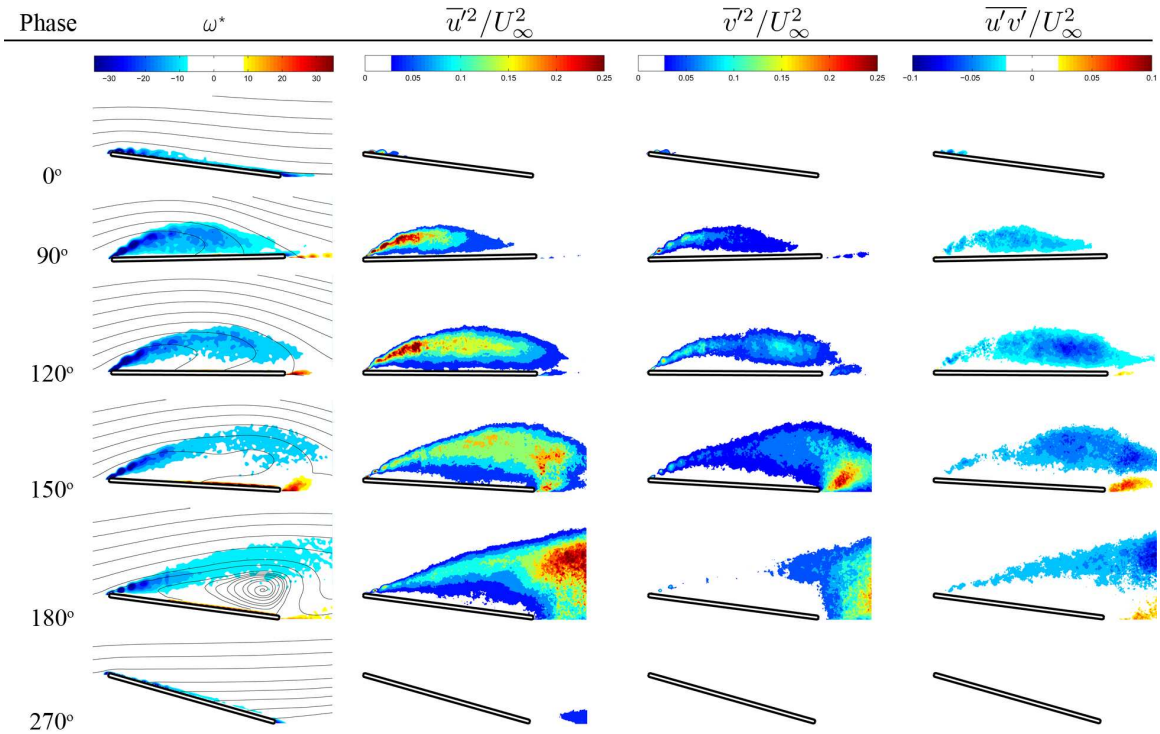

Figure B.3. Turbulence statistics for pitching and plunging flat plate at $Re = 30,000$

Acknowledgments

The work has been supported by the Air Force Office of Scientific Research's Multidisciplinary University Research Initiative (MURI) and by the Michigan/AFRL (Air Force Research Laboratory)/Boeing Collaborative Center in Aeronautical Sciences.

References

[1]Shyy, W., Lian, Y., Tang, J., Viieru, D., and Liu, H., *AErodynamics of Low Reynolds Number Flyers*, Cambridge University Press, 2008.

[2]Ol, M. V., Bernal, L. P., Kang, C., and Shyy, W., "Shallow and deep dynamic stall for flapping low Reynolds number airfoils," *Experiments in Fluids*, Vol. 46, No. 5, 2009, pp. 883–901.

[3]McCroskey, W., Carr, L., and McAlister, K., "Dynamic Stall Experiments on Oscillating Airfoils," *AIAA J.*, Vol. 14, No. 1, 1976, pp. 57–63.

[4]Kang, C., Aono, H., Trizila, P., Baik, Y., Rausch, J., Bernal, L., Ol, M., and Shyy, W., "Modeling of Pitching and Plunging Airfoils of Reynolds Number between 1x10^4 and 6x10^4," *27th AIAA Applied Aerodynamics Conference*, AIAA-2009-4100, San Antonio, TX, 2009.

[5]Ol, M. V., McAuliffe, B. R., Hanff, E. S., Scholz, U., and Kaehler, C., "Comparison of Laminar Separation Bubble Measurements on a Low Reynolds Number Airfoil in Three Facilities," *35th AIAA Fluid Dynamics Conference and Exhibit*, AIAA-2005-5149, Toronto, ON, 2005.

[6]Kang, C. K., Baik, Y. S., Bernal, L. P., Ol, M. V., and Shyy, W., "Fluid Dynamics of Pitching and Plunging Airfoils of Reynolds Number between 1x10^4 and 6x10^4," *47th AIAA Aerospace Sciences Meeting and Exhibit*, AIAA-2009-536, Orlando, FL, 2009.